

Copyright

by

Michele Judith Young

2000

Performance of Headed Reinforcing Bars in CCT Nodal Regions

by

Michele Judith Young, B.S.C.E.

Thesis

Presented to the Faculty of the Graduate School of

The University of Texas at Austin

in Partial Fulfillment

of the Requirements

for the Degree of

Master of Science in Engineering

The University of Texas at Austin

August 2000

Performance of Headed Reinforcing Bars in CCT Nodal Regions

Approved by

Supervising Committee:

John E. Breen

James O. Jirsa

Dedication

To my mother

Acknowledgements

I would like to thank Dr. John E. Breen and Dr. James O. Jirsa for their guidance on the project and good example as professors and people. I have learned immeasurably through this research endeavor from their direction, thoroughness, and patience. Their enthusiasm and suggestions throughout this study have been immeasurable.

I would like to thank M. Keith Thompson, the Ph.D. student for this study. His helpfulness, dedication, and superb way of presenting data taught me an incredible amount. I also extend my thanks to Tony Ledesma, the other M.S. student on the research team. I could not have completed this project without his great sense of humor and tremendous amount of help in the lab and classroom. The staff of the Ferguson Structural Engineering Laboratory was invaluable in the completion of my research as well as my fellow students who helped me in many ways.

I extend special thanks to Dean VanLanduyt and the Texas Department of Transportation for sponsoring the study. Additional thanks to Headed Reinforcement Corporation and Erico, Inc., who provided the headed reinforcement used in this research.

My warmest gratitude to Paul Ziehl, whose guidance, support, patience, and selflessness are only surpassed by his wit and charm. Thanks for the entertaining remarks to keep me smiling, the pleasant company in the lab at the

wee hours of the night, and for being my closest friend. Thank you for making the mountains turn into foothills.

I would like to thank Mom and Dad, Maria, Michael, and Matthew -- the best family in the world. I appreciate the faith they had in me and support they gave me. I thank them for wonderful memories, great fun, and that I can be so proud of them. I would particularly like to thank my mother. Of all the people I have ever encountered, she is the best example of how beautiful a person can be. Her global insights, humorous thoughts, tireless support, and unconditional love helped me finish graduate school. This is just a small fraction of for what I am grateful to her. She is my role model and dear friend.

August 18, 2000

Abstract

Performance of Headed Reinforcing Bars in CCT Nodal Regions

Michele Judith Young, M.S.E.

The University of Texas at Austin, 2000

Supervisor: John E. Breen

The use of headed reinforcement in concrete bridge applications offers a partial solution to congestion and anchorage problems. Heads eliminate the need for standard hooks and can reduce straight-bar anchorage lengths. Use of headed bars is not widespread due to the lack of coverage in provisions. Common use of headed bars is not likely until satisfactory provisions are developed.

This research explored the performance of headed reinforcement in compression-compression-tension (CCT) nodal regions. Fifteen tests were performed on specimens with varying head size, head shape, specimen width, and base plate length. Mode of failure, failure load, deflection under the load point, slip of the bar, strain along the bar, and crack patterns were analyzed to determine trends in behavior.

Table of Contents

ACKNOWLEDGEMENTS	v
ABSTRACT	vii
LIST OF TABLES	xiii
LIST OF FIGURES	xiv
CHAPTER 1: BACKGROUND AND INTRODUCTION	1
1.1 General Background.....	1
1.1.1 Strut-and-Tie Modeling (STM).....	3
1.1.2 Headed Bars	3
1.1.3 Applications of STM and Headed Reinforcement	8
1.2 Literature Review	13
1.2.1 Schlaich	13
1.2.2 Bergmeister	15
1.2.3 Lormanometee.....	16
1.2.4 Armstrong	17
1.2.5 Barton	18
1.2.6 DeVries	19
1.2.7 Bashandy	20
1.3 Current Code and Specification Provisions	21
1.3.1 ACI 318 Building Code	21
1.3.2 CB-30 (ACI 318).....	21

1.3.3 AASHTO LRFD Specification	22
1.3.4 AASHTO Segmental Concrete Bridge Guide Specifications	22
1.3.5 FIP Recommendations 1996	22
1.3.6 ASTM Standards	23
1.4 Overall Goals of University of Texas at Austin Project 1855.....	23
1.5 Goals of Research Relating to This Thesis	25
1.6 Organization of Thesis	26
CHAPTER 2: RESEARCH PLAN.....	27
2.1 Objectives and Plan.....	27
2.1.1 Variables	27
2.2 Test Nomenclature	28
2.3 Selection of the Test Specimen	31
2.3.1 Basic Specimen Layout.....	31
2.3.2 Dimensions.....	39
2.3.3 Reinforcing Bars and Stirrup Layout	39
2.3.4 Specimen Details.....	39
2.4 Construction and Formwork.....	41
2.4.1 Formwork Design.....	41
2.4.2 Construction of Reinforcing Cage	44
2.4.3 Concreting	44
2.4.3.1 Weather Conditions.....	44
2.4.4 Curing.....	46

2.5 Test Setup	46
2.6 Instrumentation.....	51
2.6.1 Strain Gages	51
2.6.2 Linear Potentiometers	53
2.6.3 Slip Wire – String Potentiometer	53
2.6.4 Load Cell – Hydraulic Ram	59
2.6.4.1 Load Cell – Hydraulic Ram Calibrations.....	59
2.6.5 Data Acquisition System.....	62
2.6.5.1 Data Acquisition System Calibrations	62
2.7 Materials.....	62
2.7.1 Concrete	62
2.7.2 Reinforcing Steel.....	63
2.7.3 Type of Head.....	63
CHAPTER 3: TEST RESULTS	67
3.1 Description of Typical Test.....	67
3.1.1 Loading – Increments and Failure.....	67
3.1.2 Modes of Failure	67
3.1.1 Cracking Observed.....	68
3.1.3.1 Anchorage Failure	68
3.1.3.2 Anchorage – Yielding Failure	69
3.1.3.3 Yielding Failure	71

3.2 Test Results for All Specimens	71
3.2.1 Anchorage Failure Specimens.....	76
3.2.1.1 CCT-#8-0.00X-6-U-4-S-1.....	76
3.2.1.2 CCT-#8-0.80C-6-U-4-S-1	81
3.2.2 Anchorage – Yielding Failure Specimens.....	85
3.2.2.1 CCT-#8-0.00X-8-U-6-S-1.....	85
3.2.2.2 CCT-#8-0.80C-8-U-6-S-1	89
3.2.2.3 CCT-#8-11.68S-8-U-6-S-1	93
3.2.2.4 CCT-#8-0.00X-6-U-6-S-1.....	97
3.2.2.5 CCT-#8-5.34R-6-U-6-S-1	101
3.2.2.6 CCT-#8-0.00X-6-U-6-S-2.....	105
3.2.2.7 CCT-#8-2.17S-6-U-4-S-1	109
3.2.2.8 CCT-#8-3.23R-6-U-4-S-1	113
3.2.2.9 CCT-#8-0.00H-6-U-4-S-1.....	117
3.2.2.10 CCT-#8-3.00X-6-U-4-S-1.....	121
3.2.3 Yielding Failure Specimens	125
3.2.3.1 CCT-#8-5.34R-8-U-6-S-1	125
3.2.3.2 CCT-#8-11.68S-6-U-6-S-1	129
3.2.3.3 CCT-#8-3.90C-6-U-4-S-1	133
CHAPTER 4: COMPARISON OF TEST RESULTS	137
4.0 Introduction	137
4.1 Head Size.....	137

4.2 Head Shape.....	144
4.3 Specimen Width	146
4.4 Base Plate Length.....	147
4.5 Slip Activity	150
4.6 Measured Bar Strains	152
4.7 Development Length and Determination of a Critical Section	160
4.8 Ultimate Capacity.....	163
4.8.1 Comparison with ACI Building Code Development Length Equation	163
4.8.2 Comparison with AASHTO Basic Development Length Equation	165
4.8.3 Comparison with Flexure Theory	166
4.8.4 Comparison with DeVries Side-Blowout	170
4.8.5 Comparison with ACI Code CB-30	171
CHAPTER 5: CONCLUSIONS	177
5.1 Summary	177
5.2 Conclusions	177
5.3 Recommendations for Further Study	180
BIBLIOGRAPHY	182
VITA.....	185

List of Tables

Table 1.1 – Effective Concrete Efficiency Factors by Schlaich.....	15
Table 2.1 – Head Type Designations	29
Table 2.2 – Specimen Notation	32
Table 2.3 – Specimen Conditions	45
Table 2.4 – Concrete Mix Information.....	64
Table 2.5 – Concrete Material Properties.....	65
Table 2.6 – Steel Material Properties	65
Table 3.1 – Modes of Failure	76
Table 4.1– Comparison of Stress in Bar from Development Length.....	168
Table 4.2– Failure Load Comparison for All Specimens.....	169

List of Figures

Figure 1.1 – Head Fastening Methods	6
Figure 1.2 – Force Transfer on Straight Reinforcing Bar	6
Figure 1.3 – Force Transfer for Headed Bar	7
Figure 1.4 – Column-Footing Connection	9
Figure 1.5 – Closure Strip Details	10
Figure 1.6 – Knee Joint Details	10
Figure 1.7 – Dapped Beam Details	11
Figure 1.7(a) – PCI Recommended Dapped End Reinforcing Details	11
Figure 1.7(b) – Headed Bar Details	11
Figure 1.7(c) – STM	11
Figure 1.8 – Precast Segment Deviation Blocks	12
Figure 1.9 – Strut-and-Tie Models	14
Figure 2.1 – Head Types and Net Area of Head to Net Area of Bar Ratio	30
Figure 2.2 – Typical Nonheaded Bar Control Specimen with Reinforcement Details and Loading Conditions	33
Figure 2.3 – Typical Headed Bar Specimen with Reinforcement Details and Loading Conditions	34
Figure 2.4 – Hooked Specimen CCT-#8-0.00H-6-U-4-S-1 with Reinforcement Details and Loading Conditions	35
Figure 2.5 – Hooked Specimen CCT-#8-3.00H-6-U-4-S-1 with Reinforcement Details and Loading Conditions	36

Figure 2.6 – CCT Nodal Region	38
Figure 2.7 – Far End of Bar with Welded 5” Piece.....	40
Figure 2.8 – Reinforcement in Forms Before Casting	40
Figure 2.9 – Example of Compression Strut Dimensions.....	42
Figure 2.10 – Forms Before Casting	43
Figure 2.11 – Forms for Hooked Bar Specimens.....	43
Figure 2.12 – Typical Specimen Test Setup, Setup Group 1	48
Figure 2.13 – Welded-roller Support	48
Figure 2.14 – True Roller Support	49
Figure 2.15 – Load Setup Horizontal Spacing	49
Figure 2.16 – Typical Test Setup, Setup Group 2.....	50
Figure 2.17 – Typical Test Setup, Setup Group 3.....	50
Figure 2.18 – Slip Linear Potentiometer Setup.....	52
Figure 2.19 – Slip Wire and String Potentiometer Setup.....	52
Figure 2.20 – Strain Gage Location for Nonheaded Bar, Batch 1	54
Figure 2.21 – Strain Gage Location, Batch 1	54
Figure 2.22 – Strain Gage Location for Nonheaded Bar, Batch 2	55
Figure 2.23 – Strain Gage Location, Batch 2.....	55
Figure 2.24 – CCT-#8-0.00H-6-U-4-S-1, Batch 2	56
Figure 2.25 – CCT-#8-3.00H-6-U-4-S-1, Batch 2	57
Figure 2.26 – Slip Potentiometer Setup	58
Figure 2.27 – Side View of Deflection Linear Potentiometer Setup	58
Figure 2.28 – Slip Wire with String Potentiometer for Hooked Specimen.....	60

Figure 2.29 – Load Cell Calibration.....	60
Figure 2.30 – Load Cell and Ram Setup.....	61
Figure 2.31 – Manual Hydraulic Pump.....	61
Figure 2.32 – Concrete Compressive Strength Curves	64
Figure 2.33 – Stress-strain Curve for #8 Bars.....	66
Figure 2.34 – Typical Shear Reinforcement	66
Figure 3.1 – Crack Development for Anchorage Failure of 0.80C Forged Head Bar Specimen	70
Figure 3.1(a) – First Cracking.....	70
Figure 3.1(b) – Additional Flexural Cracking.....	70
Figure 3.1(c) – Splitting Cracks	70
Figure 3.1(d) – Shear Cracking.....	70
Figure 3.1(e) – Additional Cracking	70
Figure 3.1(f) – Anchorage Failure.....	70
Figure 3.2 – Crack Development for Anchorage-Yielding Failure of 0.80C Forged Head Bar Specimen.....	72
Figure 3.2(a) – Unloaded Beam	72
Figure 3.2(b) – Flexural Cracking.....	72
Figure 3.2(c) – Tensile Cracking Along the Compression Strut.....	72
Figure 3.2(d) – Anchorage-Yielding Failure.....	72
Figure 3.3 – Crack Development for Anchorage-Yielding Failure of No Head Bar Specimen	73
Figure 3.3(a) – Flexural Cracking.....	73

Figure 3.3(b) – Splitting and Shear Cracks	73
Figure 3.3(c) – Extensive Splitting Cracks, Anchorage-Yielding Failure	73
Figure 3.4 – Crack Development for Yielding Failure of Circular Threaded Head Bar Specimen	74
Figure 3.4(a) – Flexural Cracking	74
Figure 3.4(b) – Splitting and Shear Cracks	74
Figure 3.4(c) – Extensive Splitting Cracks	74
Figure 3.4(d) – Yielding Failure	74
Figure 3.5 – Deflection Under Load Point for CCT-#8-0.00X-6-U-4-S-1	78
Figure 3.6 – Slip of Main Reinforcing Bar for CCT-#8-0.00X-6-U-4-S-1.....	78
Figure 3.7 – Load Versus Microstrain for CCT-#8-0.00X-6-U-4-S-1	79
Figure 3.8 - Failure of South Side of Beam for CCT-#8-0.00X-6-U-4-S-1.....	79
Figure 3.9 – Post-Failure Cracking Patterns on North Side of Beam for CCT-#8-0.00X-6-U-4-S-1	79
Figure 3.10 – Failure of North Side of Beam, Stress Along Bar, and Strut-and- Tie Model Schematic for –CCT-#8-0.00X-6-U-4-S-1.....	80
Figure 3.11 – Deflection Under Load Point for CCT-#8-0.80C-6-U-4-S-1	82
Figure 3.12 – Slip of Main Reinforcing Bar for CCT-#8-0.80C-6-U-4-S-1.....	82
Figure 3.13 – Load Versus Microstrain for CCT-#8-0.80C-6-U-4-S-1	83
Figure 3.14 - Failure of South Side of Beam for CCT-#8-0.80C-6-U-4-S-1	83
Figure 3.15 – Failure of North Side of Beam, Stress Along Bar, and Strut-and- Tie Model Schematic for –CCT-#8-0.80C-6-U-4-S-1	84
Figure 3.16 – Deflection Under Load Point for CCT-#8-0.00X-8-U-6-S-1	86

Figure 3.17 – Load Versus Microstrain for CCT-#8-0.00X-8-U-6-S-1	87
Figure 3.18 - Failure of South Side of Beam for CCT-#8-0.00X-8-U-6-S-1	87
Figure 3.19 – Failure of North Side of Beam, Stress Along Bar, and Strut-and- Tie Model Schematic for – CCT-#8-0.00X-8-U-6-S-1	88
Figure 3.20 – Deflection Under Load Point for CCT-#8-0.80C-8-U-6-S-1	90
Figure 3.21 – Slip of Main Reinforcing Bar for CCT-#8-0.80C-8-U-6-S-1	90
Figure 3.22 – Load Versus Microstrain for CCT-#8-0.80C-8-U-6-S-1	91
Figure 3.23 - Failure of South Side of Beam for CCT-#8-0.80C-8-U-6-S-1	91
Figure 3.24 – Failure of North Side of Beam, Stress Along Bar, and Strut-and- Tie Model Schematic for –CCT-#8-0.80C-8-U-6-S-1	92
Figure 3.25 – Deflection Under Load Point for CCT-#8-11.68S-8-U-6-S-1	94
Figure 3.26 – Slip of Main Reinforcing Bar for CCT-#8-11.68S-8-U-6-S-1.	94
Figure 3.27 – Load Versus Microstrain for CCT-#8-11.68S-8-U-6-S-1	95
Figure 3.28 - Failure of South Side of Beam for CCT-#8-11.68S-8-U-6-S-1	95
Figure 3.29 – Failure of North Side of Beam, Stress Along Bar, and Strut-and- Tie Model Schematic for –CCT-#8-11.68S-8-U-6-S-1	96
Figure 3.30 – Deflection Under Load Point for CCT-#8-0.00X-6-U-6-S-1	98
Figure 3.31 – Load Versus Microstrain for CCT-#8-0.00X-6-U-6-S-1	99
Figure 3.32 - Failure of South Side of Beam for CCT-#8-0.00X-6-U-6-S-1	99
Figure 3.33 – Failure of North Side of Beam, Stress Along Bar, and Strut-and- Tie Model Schematic for – CCT-#8-0.00X-6-U-6-S-1	100
Figure 3.34 – Deflection Under Load Point for CCT-#8-5.34R-6-U-6-S-1	102
Figure 3.35 – Slip of Main Reinforcing Bar for CCT-#8-5.34R-6-U-6-S-1	102

Figure 3.36 – Load Versus Microstrain for CCT-#8-5.34R-6-U-6-S-1	103
Figure 3.37 - Failure of South Side of Beam for CCT-#8-5.34R-6-U-6-S-1	103
Figure 3.38 – Failure of North Side of Beam, Stress Along Bar, and Strut-and-Tie Model Schematic for – CCT-#8-5.34R-6-U-6-S-1	104
Figure 3.39 – Deflection Under Load Point for CCT-#8-0.00X-6-U-6-S-2	106
Figure 3.40 – Slip of Main Reinforcing Bar for CCT-#8-0.00X-6-U-6-S-2.....	106
Figure 3.41 – Load Versus Microstrain for CCT-#8-0.00X-6-U-6-S-2.....	107
Figure 3.42 - Failure of South Side of Beam for CCT-#8-0.00X-6-U-6-S-2.....	107
Figure 3.43 – Failure of North Side of Beam, Stress Along Bar, and Strut-and-Tie Model Schematic for – CCT-#8-0.00X-6-U-6-S-2.....	108
Figure 3.44 – Deflection Under Load Point for CCT-#8-2.17S-6-U-4-S-1	110
Figure 3.45 – Slip of Main Reinforcing Bar for CCT-#8-2.17S-6-U-4-S-1.	110
Figure 3.46 – Load Versus Microstrain for CCT-#8-2.17S-6-U-4-S-1	111
Figure 3.47 - Failure of South Side of Beam for CCT-#8-2.17S-6-U-4-S-1	111
Figure 3.48 – Failure of North Side of Beam, Stress Along Bar, and Strut-and-Tie Model Schematic for – CCT-#8-2.17S-6-U-4-S-1	112
Figure 3.49 – Deflection Under Load Point for CCT-#8-3.23R-6-U-4-S-1	114
Figure 3.50 – Slip of Main Reinforcing Bar for CCT-#8-3.23R-6-U-4-S-1.....	114
Figure 3.51 – Load Versus Microstrain for CCT-#8-3.23R-6-U-4-S-1	115
Figure 3.52 - Failure of South Side of Beam for CCT-#8-3.23R-6-U-4-S-1	115
Figure 3.53 – Failure of North Side of Beam, Stress Along Bar, and Strut-and-Tie Model Schematic for – CCT-#8-3.23R-6-U-4-S-1	116
Figure 3.54 – Deflection Under Load Point for CCT-#8-0.00H-6-U-4-S-1	118

Figure 3.55 – Load Versus Microstrain for CCT-#8-0.00H-6-U-4-S-1	119
Figure 3.56 - Failure of South Side of Beam for CCT-#8-0.00H-6-U-4-S-1	119
Figure 3.57 – Failure of North Side of Beam, Stress Along Bar, and Strut-and-Tie Model Schematic for – CCT-#8-0.00H-6-U-4-S-1	120
Figure 3.58 – Deflection Under Load Point for CCT-#8-3.00H-6-U-4-S-1	122
Figure 3.59 – Load Versus Microstrain for CCT-#8-3.00H-6-U-4-S-1	123
Figure 3.60 - Failure of South Side of Beam for CCT-#8-3.00H-6-U-4-S-1	123
Figure 3.61 – Failure of North Side of Beam, Stress Along Bar, and Strut-and-Tie Model Schematic for – CCT-#8-3.00H-6-U-4-S-1	124
Figure 3.62 – Deflection Under Load Point for CCT-#8-5.34R-8-U-6-S-1	126
Figure 3.63 – Slip of Main Reinforcing Bar for CCT-#8-5.34R-8-U-6-S-1	126
Figure 3.64 – Load Versus Microstrain for CCT-#8-5.34R-8-U-6-S-1	127
Figure 3.65 - Failure of South Side of Beam for CCT-#8-5.34R-8-U-6-S-1	127
Figure 3.66 – Failure of North Side of Beam, Stress Along Bar, and Strut-and-Tie Model Schematic for – CCT-#8-5.34R-8-U-6-S-1	128
Figure 3.67 – Deflection Under Load Point for CCT-#8-11.68S-6-U-6-S-1	130
Figure 3.68 – Slip of Main Reinforcing Bar for CCT-#8-11.68S-6-U-6-S-1.	130
Figure 3.69 – Load Versus Microstrain for CCT-#8-11.68S-6-U-6-S-1	131
Figure 3.70 - Failure of South Side of Beam for CCT-#8-11.68S-6-U-6-S-1	131
Figure 3.71 – Failure of North Side of Beam, Stress Along Bar, and Strut-and-Tie Model Schematic for – CCT-#8-11.68S-6-U-6-S-1	132
Figure 3.72 – Deflection Under Load Point for CCT-#8-3.90C-6-U-4-S-1	134
Figure 3.73 – Slip of Main Reinforcing Bar for CCT-#8-3.90C-6-U-4-S-1	134

Figure 3.74 – Load Versus Microstrain for CCT-#8-3.90C-6-U-4-S-1	135
Figure 3.75 - Failure of South Side of Beam for CCT-#8-3.90C-6-U-4-S-1	135
Figure 3.76 – Failure of North Side of Beam, Stress Along Bar, and Strut-and-Tie Model Schematic for – CCT-#8-3.90C-6-U-4-S-1	136
Figure 4.1 – Failure Loads for 8” Wide Specimens, $f'_c=2800$ psi	138
Figure 4.2 – Normalized Failure Loads w/r/t Control Specimen for 8” Wide Specimens, $f'_c=2800$ psi.....	138
Figure 4.3 – Failure Loads for 6” Wide Specimens, $f'_c=2800$ psi	140
Figure 4.4 – Normalized Failure Loads w/r/t Control Specimen for 6” Wide Specimens, $f'_c=2800$ psi.....	140
Figure 4.5 – Failure Loads for 6” Wide Specimens, $f'_c=3990$ psi	142
Figure 4.6 – Adjusted Failure Loads for 6” Wide Specimens, $f'_c=3990$ psi.....	142
Figure 4.7 – Failure Loads Adjusted w/r/t Yield Strength and Normalized w/r/t Control Specimen for 6” Wide Specimens, $f'_c=3990$ psi	143
Figure 4.8 – Failure Mode, Failure Load, and Head Comparison for All Specimens.....	145
Figure 4.9 – Clear Covers and Orientation of Headed Bars.....	146
Figure 4.10 – Failure Comparison w/r/t Width of Specimen	148
Figure 4.11 – Normalized Failure Width Comparison w/r/t 6” Wide Specimens.....	148
Figure 4.12 – Base Plate Length Failure Comparison	149
Figure 4.12(a) – Failure Loads	149

Figure 4.12(b) – Normalized Failure Comparison w/r/t the 4” Base Plate	
Specimens.....	149
Figure 4.13 – Slip at Peak Load	151
Figure 4.14 – Slip Before Total Loss of Capacity.....	151
Figure 4.15 – Force in the Bar at which 0.005” Slip or No Slip Occurred	153
Figure 4.16 – Percentage of Peak Load at which 0.005” Slip Occurred.....	153
Figure 4.17 – Force at the Support at which 0.010” Slip Occurred	154
Figure 4.18 – Force in the Bar at which 0.040” Slip Occurred.....	154
Figure 4.19 – Microstrain for the 8” Wide Specimens, $f'_c=2800$ psi.....	156
Figure 4.20 – Microstrain for the 6” Wide Specimens, $f'_c=2800$ psi.....	156
Figure 4.21 – Microstrain for the 6” Wide Specimens, $f'_c=3990$ psi.....	159
Figure 4.22 – Microstrain for the Hooked Bar Specimens, $f'_c=3990$ psi.....	159
Figure 4.23 – Specimen Possible Critical Sections.....	162
Figure 4.24 – Failure Area for DeVries Side-Blowout	171
Figure 4.25 – Determination of A_N , ACI CB-30.....	175
Figure 4.26 – Determination of A_{No} , ACI CB-30	175

CHAPTER 1: BACKGROUND AND INTRODUCTION

1.1 GENERAL BACKGROUND

Reinforced concrete bridges have a large variety of geometric or static discontinuities, that is, areas where strains are significantly nonlinear. Some examples of geometrical discontinuities are dapped ends, deviator blocks, frame corners, regions with openings, or abrupt changes of section. Statical discontinuities are found at locations where concentrated loads are applied, such as beam supports, corbels, and cable anchorages. Discontinuities pose significant theoretical and practical design and construction difficulties.

Reinforced concrete structures can be simplified by using strut-and-tie modeling theory. In strut-and-tie modeling, beam or Bernoulli regions (B-regions) and discontinuity regions (D-regions) can be used to describe the state of stress and strain in the elements. In Bernoulli or beam regions, plane strain distribution is assumed to be valid. Codes and specifications cover the design of B-regions with almost inflated accuracy [1]. However, regions of concrete structures containing discontinuities are designed rather nebulously by using standard details, rules of thumb, or past experience. There is a lack of experimental data for typical D-region applications, and therefore, minimal design guidelines have been developed. D-regions pose theoretical difficulties for designers because they usually involve multi-axial stress states due to loading by combinations of shear, moment, and torsion.

On the practical side, there are difficulties with construction of D-regions in concrete bridges. D-regions typically require large amounts of reinforcing steel to be placed in small volumes of concrete. In addition, most D-regions are overdesigned due to the lack of design provision guidance. Therefore, even greater quantities of reinforcing steel are required in an already overcrowded situation. In addition to congestion problems, the large scale of bridges often requires large-scale reinforcing bars. The use of large diameter bars creates serious development and splice problems. Straight bar anchorages and lap splices are often so long that the resulting dimensions of elements are prohibitively large. The traditional solution to problems of length is to use hooked bars or to incorporate mechanical connectors to insure development of the reinforcement. Both options have appreciable drawbacks in bridge structures, however. Hooked bars create congestion problems due to both the large sizes required and the shape. This makes fabrication of reinforcement cages and concrete placement and consolidation difficult. Mechanical connectors require special construction operations and careful attention to tolerances.

In summary, D-regions of transportation structures pose significant theoretical and practical difficulties for designers and contractors. The major theoretical difficulty of designing a transportation structure D-region is that there is little information available with which to accurately model and design a D-region. The major practical difficulty of designing a transportation structure D-region is overcoming the congestion problems and problems of reinforcement development length that usually accompany D-region construction.

1.1.1 STRUT-AND-TIE MODELING (STM)

STM offers a solution to the theoretical difficulty of modeling the behavior of D-regions. It is the method of modeling employed in this project. STM is a static or lower bound plasticity solution. The plasticity theory behind STM provides a rational basis for the method [2]. STM theory provides a good conceptual basis for the designer because it encourages the visualization of the flow of forces through a structure. In addition, the visual models reveal weak points in structures that may go undetected when merely using standard design procedures. The design of D-regions is usually not adequately addressed in codes and specifications, but STM offers a transparent methodology for the design of D-regions. All parts of the structure are of similar importance, and STM can provide a consistent level of accuracy for the entire structure because it is applicable to both B- and D-regions. However, STM is not practical for B-regions because traditional methods are simpler and faster.

See Schlaich et al.[1] for a brief overview and some examples of STM.

1.1.2 HEADED BARS

Historically, offshore oil platforms were the first to commonly use headed reinforcement [3, 4, 5]. This is due to the extremely large bar sizes required, the high volume of reinforcement required, and the ease of construction that occurs when standard hooks can be eliminated from design. Large heads were used to anchor stirrups to fully develop them over their total length. Although headed

reinforcement is widely used in the offshore oil industry, it is known that the use of headed reinforcement developed for those structures is not optimal for other applications. Large sizes and shapes of heads were conservatively chosen when the offshore industry first began utilizing headed reinforcement. There was little attention paid to optimizing the size and shape of headed reinforcement. The heads currently used generally remain the same as those used initially in the large offshore platforms.

The use of headed reinforcement in high strength concrete bridge applications offers a partial solution to the practical difficulty of congestion and problems of anchorage in D-regions. Heads eliminate the need for standard hooks and can reduce long splice or straight-bar anchorage lengths. In addition, headed reinforcement offers an easy solution for some casting procedures during construction. These include the combination of precast and cast-in-place elements and the unusual details found in many innovative bridge systems. These bridge systems include segmental, precast, and cable stay, where conditions are typically difficult to solve using straight or bent bar anchorage details. There is increasing use of headed bars in transportation structures. However, widespread use of headed bars in bridges, buildings, and traditional reinforced concrete construction has been hampered by lack of coverage in codes and specifications. Common use of headed bars by designers is not likely until data is obtained to support development of provisions that will insure satisfactory performance. The implementation of headed reinforcement seems feasible when evaluating the success of similar mechanical devices such as anchor bolts and shear studs.

There are several methods for fastening heads to reinforcing bars. This project used heads that were fastened to the bars by friction-welding, forging, or threading. Bars with heads fastened by each method are shown in **Figure 1.1**. Friction-welding involves spinning the head plate at a high speed and then pressing the bar into the spinning head. Enough heat is created from the contact of metals to weld the two parts together. A new development over the last several years is the forging of heads to bars. The forging process can be done quickly in the field with the bars in place at a cost of approximately \$2/head. The simplicity of the forging process and the compactness of the forged heads make this type of headed bar particularly attractive for anchorage and continuity detailing. The third method for fastening heads to bars is by threading the bars and heads. Fastening can be done with ease in the field or in the manufacturing plant.

Both plain and deformed bars can be used in applications. However, in this study, only deformed headed bars were used. Stresses propagating through reinforced concrete can be transferred to the reinforcing bars by bearing on the deformations, also called lugs, as shown in **Figure 1.2**. The use of headed deformed bars introduces a large bearing area, thus reducing dependency on transfer of stresses along the deformed bar. The method of force transfer characteristic of headed bars is shown in **Figure 1.3**. Because the headed bar transfers force primarily through bearing, large bar forces can be developed in very short embedment lengths.

INSERT 1.1, 1.2

INSERT 1.3

1.1.3 APPLICATIONS OF STM AND HEADED REINFORCEMENT

Possible uses for headed reinforcement in highway structures are shown in the following figures. **Figure 1.4** shows a column-footing connection using hooked bars and conventional lap splicing compared with one in which headed bars are used. Details of a closure strip between precast units or in staged construction are shown in **Figure 1.5**. Improved confinement and anchorage conditions would be anticipated using headed bars in a knee-joint, as shown in **Figure 1.6**. Headed bars would further simplify dapped end reinforcement, as shown in **Figure 1.7**. The dapped beam also illustrates the advantages of headed bars for developing forces at nodes in STM. A very congested zone in segmental construction is the deviator block. Details using conventional and headed reinforcement are shown in **Figure 1.8**.

INSERT FIGURE 1.4

INSERT PICTURE 1.5 AND FIGURE 1.6

INSERT FIGURE 1.7

INSERT FIGURE 1.8

1.2 LITERATURE REVIEW

1.2.1 SCHLAICH [1]

The need for a uniform design concept applicable to all parts of the structure is met by STM. STM offers this transparent design concept by using consistent design criteria for the design of tension and compression members with regards to safety and serviceability. STM includes conceptualizing the flow of forces throughout the structure. Several examples of STM are shown in **Figure 1.9**. The three basic elements of STM are struts, ties, and nodes. Struts are the compression paths. They consist of concrete in compression and are either two or three-dimensional stress fields. The strength of the concrete in a compression field or node largely depends on its multi-axial state of stress and on disturbances from cracks and reinforcement. In **Figure 1.9**, compression struts are shown by dashed lines. These compressive stress fields are distributed and held together by tensile ties. Ties are the tension paths, which exist in the form of bonded reinforcing bars, bonded reinforcing strands, or tensile stress fields in concrete. Ties are essentially one-dimensional elements between nodes. Nodes are located where struts, ties, or combinations of struts and ties intersect and the internal forces are redirected. In **Figure 1.9**, tension ties are indicated with solid lines.

Struts and ties should be adapted to the direction and size of internal forces. Reinforcement is generally placed to take any tensile stresses that may develop. For a safe design, reinforcement should be used in all places where the tensile stresses imposed exceed the tensile strength of the concrete. Reinforced

Insert 1.9

ties are much more deformable than concrete struts. Therefore, models with the least and shortest number of ties are ideal.

Schlaich offers recommendations for determining limits of effective concrete strength. These are shown in **Table 1.1**:

Effective Concrete Strength Limits Proposed by Schlaich State of Stress and/or Reinforcement Layout for Strut or Node	f_{ce}
Undisturbed and uniaxial state of compressive stress that may exist for prismatic struts and CCC-nodes	$0.85f'_c$
Tensile strains and/or reinforcement perpendicular to the axis of the strut may cause cracking parallel to the strut with normal crack width; this applies also to nodes where reinforcement is anchored in or crossing the node.	$0.68f'_c$
Tensile strains causing skew cracks and/or reinforcement at skew angles to the strut's axis	$0.51f'_c$
For skew cracks with extraordinary crack width. Skew cracks would be expected if modeling of the struts departs significantly from the theory of elasticity's flow of internal forces. Considerable redistribution of internal forces would be required to exploit the member's ultimate capacity.	$0.34f'_c$

Table 1.1: Effective Concrete Efficiency Factors by Schlaich [3]

1.2.2 BERGMEISTER [7]

Bergmeister provides a collection of recommendations for STM nodes. He reports expressions for permissible bearing stresses of concrete confined by bearing plates. Problems in calculating allowable stresses and probable mechanics of failure are discussed. These problems are associated with the geometry of bearing plates related to the loaded surface and the plate geometry. Concrete efficiency factors from several sources for unconfined and confined CCT nodes are given. Confined CCT nodes include confinement due to shear reinforcement and exterior anchor plates.

Recommendations for geometry design of a CCT node include achieving hydrostatic stress or equal stresses on all of the node faces. Strut geometry is defined by considering geometrical constraints such as bearing plates. Strut angles associated with tension ties should fall within the range of 25 to 65 degrees to avoid excessive cracking. For unconfined nodes, a concrete efficiency factor of 0.8 is suggested as a design simplification for concrete strengths up to and including 4000 psi. It is suggested to reduce effective concrete strength in compression diagonals by an additional 0.6. This is done because most compression diagonals occur in webs of beams and girders. The web is thinner than the rest of the member. It experiences developing cracks and carries higher stresses, both which reduce effective concrete strength. This may lead to more localized failures of the concrete. The nodal zone must also fulfill minimum requirements for development length, concrete cover and bar spacing limits. He also offers recommendations on dimensioning struts, ties, and nodes with the use of hooks.

1.2.3 LORMANOMETEE [8]

A study of the effect of lateral pressure on bond strength of deformed reinforcing bars was conducted by Lormanometee at the University of Texas at Austin. Sixty pullout specimens were tested with varying concrete strength, applied lateral pressure, bar size, and distance from the face on which lateral pressure was applied to the embedded bar. The results of the tests showed that the bond strength increased with the increase of concrete compressive strength and the increase of lateral pressure. Increases in strength due to lateral pressure were

found to be larger as the volume confined was reduced. Vertical splitting was prevented when distance from the lateral pressure faces to the embedded bar was small. Therefore, the bond strength increased. However, vertical splitting was not prevented when distance from the lateral pressure faces to the embedded bar was high. Increases in bond strength due to lateral pressure were small for these specimens. Final recommendations by Lormanometee were to neglect the increase in bond strength created by lateral pressure in design guidelines. The increase in bond strength found in specimens with small distances from the lateral pressure faces to the embedded bars is neglected because such distances in most structures are larger than the 6" high specimens tested. Results from the specimens with greater distances from the lateral pressure faces to the embedded bars show no significant increase in bond strength. These specimens are more indicative of actual structures because the concrete volume was larger than that of a 6" cube used for concrete strength determination.

1.2.4 ARMSTRONG [9]

Armstrong conducted a study of sixteen scaled bent cap overhangs designed using the STM approach. The specimens were a mix of prestressed reinforcement, non-prestressed reinforcement, and combinations of the two. Headed reinforcement was used in eight of the specimens to anchor the bars in replacement of standard hooks. The headed reinforcement specimens were designed using ultimate strength for flexure and STM for shear. Headed reinforcement was only used for part of the flexural reinforcement. The use of headed reinforcement considerably improved the constructibility of the cages.

Congestion in the anchorage areas was reduced by 50 percent. Placement and consolidation of the concrete mix in anchorage areas was improved. However, there were no improvements in terms of crack control with headed reinforcement. In addition, strains in the reinforcement were negligible near the head areas, indicating that the bars were already fully developed without the contribution of the heads. The overall findings of the study were that the specimens with the best performance at costs comparable to present costs had a high percentage of prestress in the design. None of these specimens used headed reinforcement.

1.2.5 BARTON [6]

This study was an investigation of strut-and-tie models for dapped beam details. Phases two and three of the study focused on testing the nodes of the structure, as designed using STM. Among the specimens tested were ten CCT nodes with compression strut angles of 60 degrees. All CCT nodes tested were confined on the lower face by base plates of various sizes. Results of the tests indicated that STM could efficiently and effectively be used to design dapped beam details. The isolated node tests provided information on concrete performance in the compression strut and on the anchorage of reinforcement in the node. Tests showed that a decreased loaded area (determined by base plate size) resulted in increased concrete efficiency factors. Conclusions of the study compared concrete efficiency factors resulting from Barton's tests to those recommended by others. Barton's efficiency factors were consistently higher. His discussion of efficiency factors could be applicable to interpreting the results of testing done for this thesis.

1.2.6 DEVRIES [10]

Recent work at The University of Texas was aimed at providing data on basic anchorage characteristics of headed bars. Shallow and deep-embedment pullout tests were performed on over 140 headed bar specimens. Variables included embedment depth, edge distance, close spacing, corner placement, concrete strength, and head size and shape. The two failure modes of interest were pullout-cone and side-blowout. The general results showed that for low ratios of embedment depth to edge distance, pullout-cone capacity governed failure. For high ratios of embedment depth to edge distance, side blowout failure governed. Placement of the bar near an edge reduced capacity; it was further reduced by placement near a corner. Shallow embedment tests were primarily affected by embedment depth, edge distances, and concrete strength. A design equation for pullout-cone capacity was given. Anchorage strength due to development length was neglected for conservatism. Deep embedment tests placed near edges or corners failed in side blowout. They were primarily affected by edge distance, net bearing area of the head, and concrete compressive strength. Transverse reinforcement in the anchorage area did not affect ultimate capacity. Corner placement and close spacing of bars reduced the blowout capacity. An equation to predict side-blowout capacity was given. Development length was ignored for conservatism. This work showed that headed reinforcement is a viable method for providing anchorage of reinforcement in concrete members.

1.2.7 BASHANDY [11]

A study of the anchorage behavior of headed reinforcement in joints was undertaken. Basic pull-out tests were conducted. The effects of cyclic loading on head anchorage were investigated. Anchorage capacity was not significantly affected by cycling the load between 5 and 80% of the ultimate capacity. Increase in slip was minimal while in the elastic range of the headed bar. Other tests anchored the head behind crossing bars. A positive anchorage was created when the clear head dimension was at least half of the crossing bar diameter. This improved anchorage capacity by creating lateral restraint to prevent side blow-out and increasing effective bearing area of the head. Results from this portion of the testing also indicated great potential for use of headed bars in transverse reinforcement. Large-scale exterior beam-column joints were tested. Results indicate anchorage along embedment length and bearing of the head must be considered as a unit. No significant effects on anchorage capacity due to head aspect ratio and orientation were found. Anchorage capacity increased with the increase of side cover. Confinement increased bearing capacity under the head and increased ultimate load. Results from the exterior joint tests showed anchorage capacities significantly lower than those predicted with pullout tests. This difference is probably due to joint shear cracking before failure. A design equation was presented for development length required to develop yield stress in a headed bar terminating in an exterior joint. Finally, a test was conducted to compare the behavior of headed reinforcement for an exterior joint under seismic

loading to hooked reinforcement. The behavior of the headed specimen was more favorable.

1.3 CURRENT CODE AND SPECIFICATION PROVISIONS

Although headed reinforcement has been utilized for quite some time, there is minimal code and specification coverage for its usage.

1.3.1 ACI 318 BUILDING CODE [12]

The ACI 318-99 Building Code offers minimal recommendations for headed reinforcement usage. These are found in Section 12.6 Mechanical Anchorage. Any mechanical device used must fully develop the reinforcement by itself or fully develop the reinforcement in combination with the embedment length of the reinforcement without damage to the concrete. Test results must show adequacy of the anchorage device.

There are currently no guidelines for STM in the ACI Code. However, ACI Committee 318 is actively seeking ways of introducing provisions specifically for headed reinforcement.

1.3.2 CB-30 (ACI 318) [13]

This proposed code appendix provides detailed guidance for anchoring to concrete. It has been adopted to be Appendix D for the 2002 ACI Standard Building Code. Section D.5 presents requirements for tensile loading of anchors. The information presented is aimed at the usage of headed studs and post-installed anchors but may have some application to headed reinforcement.

1.3.3 AASHTO LRFD SPECIFICATION [14]

The AASHTO LRFD Specification makes minimal recommendations for headed reinforcement usage. These fall under the Bridge Specification, Section 5.11.3 Development by Mechanical Anchorages. It allows reinforcement to be entirely developed or partially developed by means of a mechanical device, as long as the concrete is not damaged. Performance of the mechanical anchorage must be verified by laboratory tests. Complete details must be shown in contract documents because standard details have not been developed.

Section 5.6.3 Strut-and-Tie Model of the Bridge Specification provides guidance in STM.

1.3.4 AASHTO SEGMENTAL CONCRETE BRIDGE GUIDE SPECIFICATIONS [15]

The AASHTO Segmental Bridge Guide Specification provides considerable guidance on STM. Section 4.2 of the Analysis section is devoted to STM. STM may be used when allowable tensile stresses are exceeded or strain distribution is nonlinear. It is to be used in B or D region design, as indicated in Section 12.4, and in the design of brackets and corbels, stated in Section 12.5. The commentary contains several design examples in Sections 12.4 and 12.5.

1.3.5 FIP RECOMMENDATIONS 1996 [16]

These recommendations offer guidance in determining the strength of ties, struts and nodes of strut-and-tie models, in addition to designing D-regions and B-regions.

When an anchor plate is used in a node, as with headed reinforcement in a CCT node, the load transfer from the tie to the struts may be regarded as a compression node. With this consideration, recommended limits from Section 5.6.2 for stress at the node face for compression nodes are:

- for biaxial compression: $f_{2cd} = 1.20 f_{1cd}$

- for triaxial compression: $f_{3cd} = 3.88 f_{1cd}$

1.3.6 ASTM STANDARDS

ASTM A 970/A 970M-98 [17] sets standards for the manufacturing of headed reinforcement. This standard stipulates that the head area must be ten times the area of the bar unless separate tests and approval are obtained for smaller sizes of heads. The current ASTM standard inhibits the widespread use of headed reinforcement by needlessly limiting the head area relative to bar area. Headed reinforcement with a smaller head area to bar area ratio than ten can still be useful. Any size of head on the end of reinforcement helps to decrease development length of the bar. It seems that ASTM should only set standards for the fabrication quality. Head size should be the responsibility of the designer.

1.4 OVERALL GOALS OF UNIVERSITY OF TEXAS AT AUSTIN PROJECT 1855

The research described above on headed anchors in reinforced concrete was designed to evaluate a particular aspect of behavior, but not overall behavior of a structure or element containing headed bars. Pull-out tests, splitting tests, fatigue tests, and tests for seismic events have been performed with headed reinforcement. However, applications with multiple headed reinforcing bars or

large-scale specimens using these anchors in typical bridge structures is lacking. Potential applications of headed reinforcement in bridge structures were identified in Section 1.1.3 of this thesis. Tests performed on specimens that mimic these applications are needed. CTR Project 1855 at the University of Texas at Austin is intended to fill some of the gaps in the body of knowledge on headed bars.

Project 1855 commenced with a feasibility study on using headed reinforcing bars in specific applications for highway structures. Initially, it was envisioned that specific highway structures would be selected for study in which complex or congested reinforcing details could be improved by substitution of headed bar anchorages for conventional hooked or straight bar anchorages. The study would have focused within a narrow scope of predetermined, specified structural elements. As planning progressed, however, a more general path of research was seen to be more desirable. Thus the research focused on applications of headed bars in generic structural details. The generic details identified for study were headed reinforcing bars in or around strut-and-tie nodal regions and lap splices. Such general information is extremely useful because it can be applied to a variety of design situations in different types of structures or details.

The long-term objective of the study is to quantify the behavior of headed reinforcing bars having a range of geometric configurations and used in various applications. The intent is to determine an appropriate (headed) mechanical anchor as a function of specimen dimensions, cover, development requirements,

and concrete strength. The results can be utilized to develop procedures for use in concrete design codes and specifications.

Some specific goals of the strut-and-tie node study of headed reinforcement are:

- a) to determine and define practical nodal boundaries. This is necessary to determine limits of critical sections for anchorage.
- b) to formulate a systematic, simple method for determining a node face area on which concrete stresses act.
- c) to determine effective concrete strength factors at the appropriate faces of the node as a function of confinement.
- d) to develop an equation or methodology for determining an adequate head size to anchor the bar.
- e) to determine the effects of confinement on head performance.
- f) to evaluate the effects of confinement on anchorage.

1.5 GOALS OF RESEARCH RELATING TO THIS THESIS

Applications of headed reinforcing bars can be visualized for a multitude of details in reinforced concrete structures. The scope of this thesis focuses on performance of headed reinforcing bar behavior in a particular STM CCT node. Variables for the fifteen exploratory tests completed were head size, head shape, specimen width, and base plate length. Specific information regarding the design of the test specimen is found in Chapter 2. A comparison of basic test information such as mode of failure, failure load, deflection under the load point,

slip of the bar, strain along the bar, and crack patterns was performed to determine trends in behavior. These test results along with future results may be used to set guidelines for the use of headed reinforcement in a CCT node. From this information, the design guidelines developed can be extrapolated to similar configurations in a variety of structures.

1.6 ORGANIZATION OF THESIS

Chapter 1 provides an introduction of the topic, necessary background information, current provisions, overall project goals, thesis goals, and a roadmap for the organization of the thesis. Chapter 2 establishes test nomenclature and describes the research plan in detail. This includes the specific objectives for the research, the test specimen design, construction, test setup, instrumentation, materials, loading history and method of test. Chapter 3 presents test results. A general description of the test is given, and data results for all specimens are summarized. Chapter 4 compares all data obtained, interprets the data, describes the significance of the test results, and compares them with current provisions. Chapter 5 summarizes the conclusions from the testing and provides recommendations for future testing.

CHAPTER 2: RESEARCH PLAN

2.1 OBJECTIVES AND PLAN

The objective of the study was to report the behavior of headed reinforcing bars compared to hooked bars and straight bars in a given CCT nodal region. CCT nodes were investigated, in which the tension ties consisted of single reinforcing bars. Exact node geometry is unknown, but it is depicted with a triangle in this thesis. These tests may aid in determining a method of defining nodal region dimensions for CCT strut-and-tie modeling. Mode of failure in relation to head size and shape was determined. Trends in behavior depending on failure load, mode of failure, head performance, and cracking pattern were noted. In the future, the test program may be expanded to beams with multiple reinforcing bars. Interaction effects between multiple bars may affect confinement, failure load, failure mode, and other behavioral patterns.

2.1.1 VARIABLES

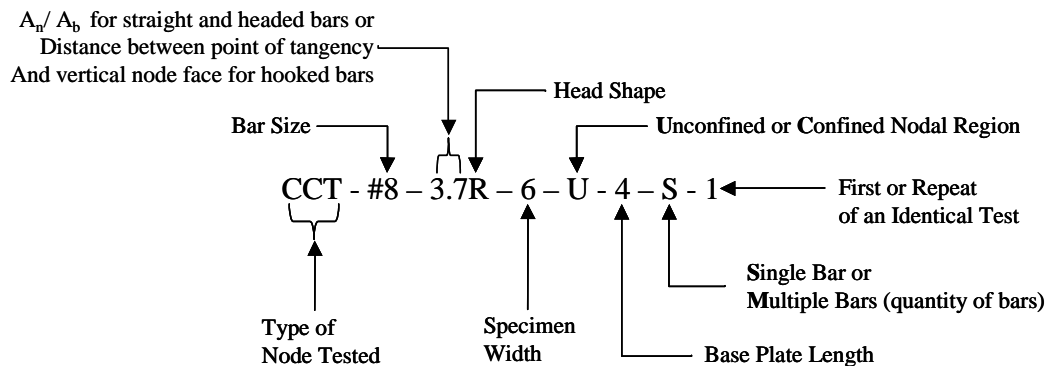
The variables considered in this thesis are the net head area to bar area ratio, the head shape, the specimen width, and the base plate length. Net head area is defined as the gross area of the head less the bar area. Fifteen specimens with varying conditions were tested and are discussed.

2.2 TEST NOMENCLATURE

Each specimen was initially given a numeric identifier describing the chronological order of testing. For analysis and reporting purposes, each

specimen was subsequently given a more descriptive, mnemonic nomenclature.

The following is an example of the notation used for specimens in this thesis:



There are nine elements in the notation, as shown above in the example. The first identifier describes the type of STM node tested. In the example, the node is a compression-compression-tension node. All tests described in this thesis were CCT nodes.

The second identifier indicates the standard bar size used as the tension tie. All tests described herein contained #8 bars.

The third identifier is the ratio between net area of the head and area of the bar for nonheaded and headed bar specimens. Net area of the head is defined as the gross area of the head less the area of the bar. For hooked bar specimens, the third identifier is the horizontal distance in inches between the back vertical face of the CCT node triangle and the point of tangency between the hooked portion and the straight portion of the standard hook bar. For specimens described in this thesis, this identifier varies from 0.00 for nonheaded straight bars to 11.68 for the 3"x3" friction-welded headed bars. For hooked bars, it varies from 0.00 to 3.00.

The fourth identifier describes head shape. A listing of head shapes and their symbolic designations is presented in **Table 2.1**.


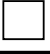



Head Type Designations		
Head Shape	Graphical Symbol	Alphanumeric Symbol
No Head		X
Square Head		S
Rectangular Head		R
Circular Head		C
Hooked Bar		H

Table 2.1: Head Type Designations

The symbol for head shape is used to graph the data obtained from the tests. The alphanumeric symbol is used to identify head shape in the notation. All head types tested in this study with their respective head area ratios are shown in **Figure 2.1**.

The fifth identifier describes specimen width in inches. The specimens were either 6 or 8 inches wide.

Insert figure 2.1

The sixth identifier indicates whether the nodal region included shear reinforcement. “U” is used when there are no stirrups in the nodal region. “C” is used when there are stirrups in the nodal region. All tests described in this thesis had unconfined nodal regions.

The seventh identifier describes the length of the base plate in the CCT nodal region in inches. The base plate in the nodal region was either 4” or 6” in length.

The eighth identifier demarcates a single flexural reinforcing bar with “S” or multiple flexural reinforcing bars with “M(#)” stating the number of bars in parentheses. All specimens described in this thesis were single bar specimens.

The ninth identifier indicates if the test is the first one of its type or a replicate of a previous test. **Table 2.2** shows specimens in chronological order of testing listed with their notation and variables.

2.3 SELECTION OF THE TEST SPECIMEN

2.3.1 BASIC SPECIMEN LAYOUT

The basic test specimen was intended to simulate a generic CCT node. The tests described in this thesis were first in a planned series. Thus the specimens were detailed in order to provide the foundations of understanding. Basic reinforcement spacing and details for nonheaded, headed, and hooked bar specimens are shown in **Figure 2.2**, **Figure 2.3**, **Figure 2.4**, and **Figure 2.5**, respectively. Each specimen had one main bar that was headed, hooked, or straight (control specimens). Points of tangency between curved and straight portions of the hooked bars are indicated with white dots. Dimensions a and b

Insert table 2.2

Figure 2.2

Figure 2.3

Figure 2.4

Figure 2.5

vary and are given in **Table 2.2**. The beginning of a nonheaded, straight bar was placed with two inches of cover to the end of the beam, as shown in **Figure 2.2**. The beginning of the reinforcing bar was placed leaving less than two inches of cover to the end of the beam for headed bars, as shown in **Figure 2.3**. For hooked bars, the least amount of cover to the end of the beam was two inches, as shown in **Figures 2.4-5**. The main reinforcement was placed along the center axis of the beam with respect to beam width. #4 reinforcing stirrups were placed at 6" on center from the loading point to the far end face of the beam. The CCT region from the load point to the end face of the beam had no reinforcing stirrups in order to observe the behavior of the nodal region without interaction of shear confinement.

Specimen geometry was chosen with the intention of creating a compression strut angle θ of around 45° . All specimens were loaded in a manner that was to provide information regarding the effective strength of the concrete in the nodal region and the anchorage due to head geometry and bearing area. An expanded view of the nodal region is shown in **Figure 2.6**. The highly compressed node is indicated by the triangular area, although its exact geometry is unknown and the overall nodal region is much larger. The node is subjected to a two-dimensional force path. The diagonal compression strut carries force from the load point to the CCT node that is formed at the base plate. The strut angle is controlled by the placement of the load point. The tension tie and vertical compression strut are needed to provide equilibrium at the node. Node geometry

insert 2.6

is controlled by width of the specimen, head geometry, and length of the bearing plate under the node.

2.3.2 DIMENSIONS

Figures 2.2-5 and **Table 2.2** give general dimensions of the beams tested for CCT node application. All headed bar specimens and straight bar control specimens were 72" in length, 20" in height, and either 6" or 8" in width. The center-to-center distance between supports for all specimens was 60". The hooked bar specimens were 77 ½ " in length. This extra length enabled the CCT node to form near the point of tangency between the curved portion and straight portion of the reinforcing bar and still maintain at least 2" of cover in the X direction. The bearing plate center-to-center distance for the hooked bar specimens was 60".

2.3.3 REINFORCING BARS AND STIRRUP LAYOUT

Reinforcing bar details are shown in **Figures 2.2-5**. A schematic of the different bar end types is shown in **Figure 2.1**. To insure proper anchorage of the far end of the reinforcing bar, a five inch piece of #8 reinforcing bar was welded to the bar perpendicular to the length of the bar, as shown in **Figure 2.7**. **Figure 2.8** provides a typical view of the reinforcement in the forms before concrete placement.

2.3.4 SPECIMEN DETAILS

All specimens have a 60" center-to-center distance between the support plates, as shown in **Figures 2.2-5**. All specimens were loaded approximately at the quarter point, with 15" measured along the length of the beam from center of

Insert 2.7, 2.8

the roller support nearest the end face of the beam to the center of the load plate. This load arrangement created a compression strut at 45° with the horizontal. The vertical compression strut starting at the top face of the beam under the load plate is assumed to be 6" in length and the full width of the beam. The diagonal face of the node created by the diagonal compression strut is assumed to be around $6\sqrt{2}$ " or 8.46" in length. The compression strut formed directly above the roller support is defined by the area of the base plate supporting the beam. In the tests described in this thesis, the strut was either 6" or 4" in length. An example of estimated compression strut dimensions for a specimen with a base plate 6" in length is shown in **Figure 2.9**. For specimen CCT-#8-0.00H-6-U-4-S-1, the CCT node was set with the vertical nodal face in line with the beginning of the straight portion of the bar, as shown in **Figure 2.4**. For specimen CCT-#8-3.00H-6-U-4-S-1, the CCT node was set with the beginning of the straight portion of the bar 3" down the bar from the node face, as shown in **Figure 2.5**. All compression strut cross-sectional areas were assumed to cover the entire width of the beam at any given point.

2.4 CONSTRUCTION AND FORMWORK

2.4.1 FORMWORK DESIGN

All formwork was made of plywood and 2x4's. Formwork was made so that the beams containing straight and headed bars could be cast upright. **Figure 2.10** shows the forms in place before casting. Forms were reused for the two separate casts. Forms for the hooked bars were made to cast the beams on their side, as shown in **Figure 2.11**. These were cast on their side to ease construction

insert 2.9

insert 2.10, 2.11

and casting. It was assumed there would be no variation in results from this. All forms were sealed with silicon caulk or duct tape to prevent leakage. To prevent bonding between the concrete and forms, all forms were sprayed with form oil before setting the reinforcement in them prior to concrete placement.

2.4.2 CONSTRUCTION OF REINFORCING CAGE

The stirrups were threaded onto the main reinforcement, spaced evenly at 6", and tied with wire to the main reinforcing bar. For the 8" wide specimens, 1¼" chairs were tied to each side of the reinforcement to position the cage in the forms. 1" chairs were tied to each side of the reinforcement for all 6" wide specimens. These chairs extended longitudinally along the beam. Two groups of three single chairs were used to support the main reinforcing bar. These groups of chairs came in contact with the bottom and side forms and were placed about one foot in from each bar end.

2.4.3 CONCRETING

The specimens for this study were cast in two batches, as indicated in **Table 2.3**.

2.4.3.1 WEATHER CONDITIONS

Concrete for beams in Batch 1 was placed in low 70 degree weather. The climate was humid for the first two casting and curing periods. Concrete for specimens in Batch 2 was placed in mid-50 degree weather, and the curing conditions were quite dry and may explain the high concrete strength of this group of specimens.

INSERT TABLE 2.3

2.4.4 CURING

Concrete for beams in Batch 1 was placed, the surface was finished and a few hours later was covered with wet burlap and plastic. Concrete for specimens in Batch 2 was placed, finished, and covered with plastic after a few hours. The concrete surface of all specimens was rewet daily. The plastic was removed about four days after casting. The caps were removed from the strength test cylinders at the same time to provide comparable curing conditions. Forms were typically removed from the specimens after one week of curing. At this time, the concrete test cylinders were demolded, as well.

2.5 TEST SETUP

Figure 2.12 shows a typical specimen and test setup. The beam is loaded downward at its quarter point. The reaction frame is bolted into the laboratory test floor. The test setup generally remained the same throughout all testing. The specimens were grouped according to small differences in test setup, as shown in **Table 2.3**. For the specimens tested in Setup Group 1, neoprene padding was placed between the reaction floor and the base plates. The base plate nearest the headed end face of the beam was either 4” or 6” in length. The base plate nearest the back end face of the beam was 12” in length for all specimens. The base plates extended the full width of the beam for specimens in all setup groups. It was discovered that there was uneven bearing upon the support base plates due to beam rotation and uneven surfaces. Therefore, specimens in Setup Group 2 were mounted on supports consisting of a neoprene pad, a round support welded to a

plate, and a 2" thick base plate grouted to the bottom of the beam. **Figure 2.13** shows a welded-roller support. Support conditions for Setup Group 3 were changed to true roller supports, and a load cell was placed under the support nearest the end face of the beam, as shown in **Figure 2.14**. These changes were made because of inconsistencies between the load measured under bearing and the load being applied were detected.

For every specimen, a plate 6" in length and the full width of the specimen was centered over the load point on the top face of the beam. Placement of the load plate varied slightly from specimen to specimen depending on the length of the base plate defining the vertical compression strut from the support to the node. The load plate was always placed so that a 45° diagonal compression strut formed. There was always a 15" center-to-center horizontal distance between the support nearest the end face of the beam and the load point as shown in **Figure 2.15**. For specimens in Setup Group 1 and Setup Group 2, the load cell and ram were placed on the beam, as shown in **Figure 2.16**. For Setup Group 3, as shown in **Figure 2.17**, the load cell was moved to a position directly under the support nearest the end face of the beam for more accurate determination of reactions.

The support nearest the end face of the beam and the dimension of the support vertical compression strut were changed from 6" to 4" for all specimens following the first one tested in Setup Group 3. The first specimen in Setup Group 3, contained a straight, nonheaded bar that failed by bar slip just before reaching yield. It was felt that subsequent tests with headed bars and hooks would fail by yielding. Therefore, the length of the bearing plate was reduced in

Insert 2.12, 2.13

insert 2.14, 2.15

Insert 2.16, 2.17

order to force the mode of failure to bar slip or crushing of the concrete rather than yielding of the steel.

2.6 INSTRUMENTATION

Strain gages, potentiometers, slip wires, and a load cell were used to monitor specimen behavior. The strain gages were affixed at specific points along the length of the headed, nonheaded, or hooked reinforcing bars. A linear potentiometer was used to detect bar slip, while the other was utilized to record downward deflection of the beam at the load point. The linear potentiometer used to detect slip extended from the end face of the beam through a copper tube cast into the specimen until coming in contact with the end of the reinforcing bar. A schematic of this setup is shown in **Figure 2.18**. For the hooked bar specimens, the differential was taken between readings from a slip wire attached to a string potentiometer and horizontal movement of the front face of the beam. **Figure 2.19** shows this setup.

2.6.1 STRAIN GAGES

All strain gages used were type EA-06-250BG-120 from Micro Measurements Group©. Each was a length of ¼ inch, had 120 ohm resistance, and a gage factor of $2.060 \pm 0.5\%$. Using a hand grinder, one inch lengths of the longitudinal rib of the bar were removed for placement of strain gages. The area where the gage was attached was sanded using 220 grit wet-dry sand paper and cleaned with acetone. The surface was then further cleaned with a mild acid solution and neutralized with a mild base solution. Strain gages were affixed to

INSERT FIGURE 2.18, 2.19

the bar surface using a two-part strain gage adhesive. They were covered with an acrylic coating, a layer of butyl rubber, and finally a quick-setting epoxy for protection during handling and concrete placement. Strain gages were affixed to the bars in the same general locations. Strain gage locations for specimens from Batch 1 are shown in **Figures 2.20-21**. Strain gage locations for all beams from Batch 2 are shown in **Figures 2.22-25**. The fourth and fifth strain gages for the straight and headed bar specimens are located on opposite sides of the bar to detect any differential in strain over the cross-section. Bars were laid in the formwork strain gage side down to prevent damage during concrete placement.

2.6.2 LINEAR POTENTIOMETERS

A 4” linear potentiometer for detection of bar slip was clamped to a support that was fastened to the front face of the concrete beam. The slip potentiometer setup is shown in **Figure 2.18**, and it can also be seen in **Figure 2.26**.

Deflection of the beam under the load point was measured with a 2” linear potentiometer. **Figure 2.27** shows the deflection potentiometer setup on a typical specimen. An additional linear potentiometer was used for measuring slip of the hooked bar specimens.

2.6.3 SLIP WIRE – STRING POTENTIOMETER

The two hooked bar specimens use slip wires and string potentiometers to measure slip of the reinforcing bars. A linear potentiometer rests on the end face of the specimen. One end of the slip wire was welded to the hooked bar at the point of tangency between the curved and straight portions of the bar. The other

INSERT 2.20, 2.21

INSERT 2.22, 2.23

INSERT 2.24

INSERT 2.25

insert 2.26, 2.27

end of the slip wire was attached to a 5” string potentiometer fixed to a wooden table. The table was loaded with weights to prevent sliding.

The relative displacement between the linear potentiometer reading and the string potentiometer reading estimated the slip of the bar. Both potentiometers were needed for this setup. If just the string potentiometer were used, determining whether movement detected was due to total beam movement or slip of the reinforcement within the beam would be difficult. A schematic of the slip wire setup is shown in **Figure 2.19**. A picture of the typical slip wire setup is shown in **Figure 2.28**. This combination of string and linear potentiometers was utilized because the curved part of the hooked bar leaves no flat end surface upon which a linear potentiometer can rest to detect slip of the bar.

2.6.4 LOAD CELL – HYDRAULIC RAM

Curves from the ram and load cell calibration are shown in **Figure 2.29**. This information shows that the load cell readings are within $\pm 2.0\%$ accuracy of the actual load.

2.6.4.1 LOAD CELL – HYDRAULIC RAM CALIBRATIONS

A 100 kip load cell with 100 ton hydraulic ram and a manual pump were used for all testing. The load cell and ram are shown in **Figure 2.30**. **Figure 2.31** shows the manual hydraulic pump used for all testing. Hydraulic ram pressure was manually recorded throughout testing as an additional check.

insert 2.28, 2.29

INSERT 2.30, 2.31

2.6.5 DATA ACQUISITION SYSTEM

The program “measure” written by National Instruments was utilized to acquire data for all specimen tests. All instrumentation were mechanically as well as electronically checked to insure proper data acquisition. Initiations of a sequence of computer data point readings were done manually. This was done instead of setting the computer to automatic data recording. The hydraulic ram was pumped manually for all tests. The pressure applied to the beam by the hydraulic ram typically decreased slightly after pumping ceased for each load cycle.

2.6.5.1 DATA ACQUISITION SYSTEM CALIBRATIONS

Prior to the beginning of each test, the accuracy of the load reading was checked through the data acquisition system. When readings indicated the system was not within the allowable standard deviation for readings, the system was troubleshot until the system check reported no errors.

2.7 MATERIALS

2.7.1 CONCRETE

All concrete was ordered from the same ready mix company. The initial set of specimens cast unfortunately produced no useful information about the behavior of CCT nodes because the concrete strength was too high. These specimens are not shown in any tables, and results from their tests are not reported in this thesis. Therefore, the lowest strength concrete available was utilized for the first and second batches reported in an attempt to produce a

concrete node failure before the bar yielded. **Table 2.4** shows the concrete mix, its proportions, strength, and casting conditions. Concretes with higher strength than those used in most of these tests are usually specified in the field.

Compressive strength – time curves from the two batches are shown in **Figure 2.32**. Concrete compressive strengths were measured using 6"x12" concrete cylinders according to ASTM C39-99 [18]. Batches 1 and 2 had identical mix parameters. Therefore, Modulus of Elasticity [19], Modulus of Rupture [20], and Standard Splitting [21] tests were performed on cylinders from Batch 2 only. Material properties of the concrete used for testing are shown in **Table 2.5**.

2.7.2 REINFORCING STEEL

The main reinforcement for all CCT node specimens was #8 bars. **Table 2.6** shows the results of material tests for the #8 reinforcing bars. **Figure 2.33** is the average stress-strain curve obtained from seven bar tests. All stirrups were fabricated from #4 bars. Rectangular hoops were used as shear reinforcement in the 8" wide specimens. Two tie legs with 180° hooks were used in the 6" wide specimens. Shear reinforcement is shown in **Figure 2.34**.

2.7.3 TYPE OF HEAD

The types of reinforcing bar heads used for the CCT node specimens were discussed in **Section 2.2** and shown in **Figure 2.1**.

insert table 2.4, figure 2.32

Insert table 2.5, table 2.6

Insert figure 2.33, 2.34

Chapter 3: Method of Test and Test Results

3.1 DESCRIPTION OF TYPICAL TEST

3.1.1 LOADING – INCREMENTS AND FAILURE

The hydraulic ram applying the load was pumped manually for every test. The load cell readings were taken with the data acquisition system, at manually chosen increments of time. The load was incremented between 3 and 5 kips with the hydraulic pressure incremented between 300 and 500 psi. Load increments were close to the low end of the range when near the cracking load or failure load of the specimen. After each increment, the ram hose was blocked, cracks were marked, crack widths were measured, and behavioral notes were recorded. Several specimens were loaded again after failure to determine the further deformation and cracking that would occur.

3.1.2 MODES OF FAILURE

Modes of failure included compression strut failure, shear failure, flexural yielding failure, and a combination of compression strut failure and shear failure. While flexural yielding is the preferred method of failure in actual structures, in these research specimens the desirable mode of failure was compression strut failure. If specimen failure was controlled by the compression strut, information about the anchorage of the head and the force developed in the head and bar could be obtained. There were a number of likenesses between shear failure and compression strut failure. Both failure modes experienced sudden failures. Cracking patterns were similar until within a few kips of failure. Cracking for

both modes indicated the formation of a diagonal compression strut. Shear failure was the second mode of failure. Generally, shear failure showed signs of slip of the main reinforcement. This slip could have occurred from partial or total debonding of the main reinforcement, weak localized concrete, or as repercussions of sudden crack formation. When debonding of the head and end of the bar occurs, shear failure is likely. This is because the end of the beam has no working reinforcement. The end of the beam containing debonded reinforcement essentially becomes an unreinforced concrete block subjected to extremely high shear loads. The third mode of failure was flexural yielding of the steel. Quantitative information about the anchorage of the head and behavior of the steel was not obtained with this mode of failure. However, this mode qualitatively showed in many cases that the head anchor prevents bar slip and enables the beam to carry more load than a beam without headed reinforcement. Some beams failed in a combination of the compression strut failure and shear failure.

3.1.3 CRACKING OBSERVED

3.1.3.1 COMPRESSION STRUT FAILURE

Figures 3.1-5 show the development of cracks for CCT - #8 - 0.80C - 8 - U - 6 - S - 1, which experienced compression strut failure. The test began with an unloaded beam, as shown in **Figure 3.1**. First cracking typically occurred when the support under the node experienced about 15-20 kips. Flexural cracking

Insert 3.1-3.5

is shown in **Figure 3.2**. Flexural cracks continued to form along the rest of the beam during the remainder of the test. **Figure 3.3** shows cracking along the compression strut. The specimen experienced compression strut failure. This is shown in **Figure 3.4**. The unloaded, failed beam is shown in **Figure 3.5**.

3.1.3.2 SHEAR FAILURE

Figures 3.6-10 show the development of cracks for CCT - #8 – 0.00X – 6 – U – 6 – S – 1, which experienced shear failure. The test began with an unloaded beam, as shown in **Figure 3.6**. Flexural cracking is shown in **Figure 3.7**. **Figure 3.8** shows splitting cracks under the load point and shear cracks toward the support. Splitting cracks usually occurred when the support under the node experienced between 25-40 kips of load. Splitting cracks indicate the beginnings of failure of bond between the concrete and steel. When this occurs, bar slip is likely. The shear cracks indicate, to some extent, the formation of a diagonal compression strut. This typically occurred when the support under the node experienced 35-50 kips of load. **Figure 3.9** shows extensive splitting cracks and sudden shear failure. The unloaded, failed beam is shown in **Figure 3.10**.

3.1.3.3 FLEXURAL YIELDING FAILURE

Figures 3.11-16 show the development of cracks for CCT - #8 – 3.90C – 6 – U – 4 – S – 1, which experienced flexural yielding failure. The test began with an unloaded beam, as shown in **Figure 3.11**. Flexural cracking is shown in **Figure 3.12**. **Figure 3.14** shows some splitting cracks and a shear crack. Cracks

widen, as shown in **Figure 3.14**. The beam fails in flexure, as shown in **Figure 3.15**. The unloaded, failed beam is shown in **Figure 3.16**.

Insert 3.6-3.10

Insert 3.11-3.16

3.1.3.4 COMBINATION FAILURE

Figures 3.17-24 show the development of cracks for CCT - #8 - 0.80C - 6 - U - 4 - S - 1, which experienced a combination of compression strut failure and shear failure. The test began with an unloaded beam, as shown in **Figure 3.17**. First cracking was observed as a flexural crack directly under the load point, as shown in **Figure 3.18**. Flexural cracks continued to form and are shown in **Figure 3.19**. Splitting cracks along the main reinforcing bar were observed, as shown in **Figure 3.20**. Shear cracking then occurred from the load point diagonally down toward the bottom of the beam a few inches in front of the base plate, as shown in **Figure 3.21**. **Figure 3.22** shows additional cracking along the diagonal strut from load point to node and from the base plate up to the node. This type of cracking usually did not occur until the support under the node reached within 2-5 kips of the failure load. **Figure 3.23** shows the beam immediately following sudden shear failure. Cracks were formed parallel to and along the upper part of the diagonal compression strut during failure, as well. This indicates the compression across the entire width of the compression strut. The majority of the cracks occurred along the lower part of the width of the compression strut. The unloaded, failed beam is shown in **Figures 3.24**.

Insert 3.17-3.20

Insert 3.21-3.24

3.2.0 TEST RESULTS FOR ALL SPECIMENS

Data obtained for all CCT node specimens tested are reported in this section. The specimens are grouped in **Table 3.1** according to mode of failure for the presentation of data. The loads presented in this data are the loads experienced by the support under the node. The nominal area of the bar was used for all stress and strain calculations. Therefore, the engineering yield stress and engineering yield strain are used in the data. Data for deflection under the load point, main reinforcing bar slip, load versus microstrain of the bar, and stress along the bar are presented in the following subsections. Some of the plots are missing strain gage readings. Several strain gages were damaged or their wires broken during the concrete castings. Strain gage data could not be presented in these cases.

Mode of Failure	Specimen	Concrete Strength (psi)	Failure Load (kips)
Compression Strut Failure	CCT - #8 - 0.80C - 8 - U - 6 - S - 1	2800	52.2
	CCT - #8 - 11.68S - 8 - U - 6 - S - 1	2800	73.0
Shear Failure	CCT - #8 - 0.00X - 8 - U - 6 - S - 1	2800	45.7
	CCT - #8 - 0.00X - 6 - U - 6 - S - 1	2800	49.2
	CCT - #8 - 5.34R - 6 - U - 6 - S - 1	2800	66.9
	CCT - #8 - 0.00X - 6 - U - 6 - S - 2	3990	53.7
	CCT - #8 - 2.17S - 6 - U - 4 - S - 1	3990	43.4
	CCT - #8 - 0.00H - 6 - U - 4 - S - 1	3990	51.8
	CCT - #8 - 3.00H - 6 - U - 4 - S - 1	3990	49.0
Flexural Yielding Failure	CCT - #8 - 5.34R - 8 - U - 6 - S - 1	2800	71.8
	CCT - #8 - 11.68S - 6 - U - 6 - S - 1	2800	58.3
	CCT - #8 - 3.23R - 6 - U - 4 - S - 1	3990	61.3
	CCT - #8 - 3.90C - 6 - U - 4 - S - 1	3990	54.7
Combination Failure	CCT - #8 - 0.00X - 6 - U - 4 - S - 1	3990	42.3
	CCT - #8 - 0.80C - 6 - U - 4 - S - 1	3990	46.7

Table 3.1: Modes of Failure

Results and test data obtained for the following specimens were not informative, and therefore are not presented in this thesis:

CCT-#8-0.00X-8-U-6-S-1 (5600 psi)

CCT-#8-0.80C-8-U-6-S-1 (5600 psi)

CCT-#8-5.34R-8-U-6-S-1 (5600 psi)

CCT-#8-11.68S-8-U-6-S-1 (5600 psi)

The concrete strength was much higher than expected for this group of specimens. The specimens lacked shear reinforcement, and two specimens failed in shear. Two specimens yielded. No information regarding effects of the heads was obtained. The lack of shear reinforcement was an oversight and the specimens cast after the first set contained shear reinforcement from the load point to the far end face of the beam. The basic layout of the specimens was repeated for Casting 2, and a lower strength concrete was used.

3.2.1 COMPRESSION STRUT FAILURE SPECIMENS

3.2.1.1 CCT-#8-0.80C-8-U-6-S-1

This specimen was made in the regular CCT configuration with 2,800 psi concrete. Main reinforcement was a single #8 bar with a forged head. The beam was 8" wide, with the nodal area unconfined by shear reinforcement. The base plate was 6" in length, and this was the first test of its kind. **Figure 3.25** shows deflection under the load point. **Figure 3.26** shows slip of the main reinforcing bar occurring at failure. The first 0.03" step in slip probably occurred due to debonding of the end of the bar. The head, then, probably anchored the bar by bearing and prevented failure. Sudden, large slip occurred when the strut failed.

Figure 3.27 presents load versus microstrain of the bar during testing. The highest loads were experienced at microstrains well under yield. This specimen failed suddenly with diagonal compression strut failure. This occurred at the maximum load of 52.2 kips. Microstrain readings did not reach yield until after failure. **Figure 3.28** shows failure of the south side of the beam. The cracks formed illustrate compression strut formation. **Figure 3.29** shows a failure picture of the north side of the beam, stress along the bar, and a schematic of the node zone. During the test, it was found that bearing on the support under the node was uneven. To insure a more uniform distribution of load over the base plate, the test setup was changed. Changes included using welded rollers and hydrostone between bearing surfaces.

Insert deflection, slip

Insert microstrain, failure

Insert stress along bar, failure

3.2.1.2 CCT-#8-11.68S-8-U-6-S-1

This specimen was made in the regular CCT configuration with 2,800 psi concrete. Main reinforcement was a single #8 bar with a 3"x3" square friction-welded head. The beam was 8" wide, with the nodal area unconfined by shear reinforcement. The base plate was 6" in length, and this was the first test of its exact kind. **Figure 3.30** shows deflection under the load point. The beam experienced a rather lengthy yield plateau. **Figure 3.31** shows slip of the main reinforcing bar. There is slight movement after first yielding is detected around 50 kips. This indicates that the head began to act after the bar started to yield. **Figure 3.32** presents load versus microstrain of the bar during testing. At 54.3 kips, the specimen showed first yielding at the fifth strain gage. All but the first gage experienced strain past yield. Although the bar was almost entirely yielded, it was anchored by the large head. The specimen failed suddenly in diagonal compression strut failure at the maximum load of 73.0 kips. **Figure 3.33** shows failure of the south side of the beam. **Figure 3.34** shows a failure picture of the north side of the beam, stress along the bar, and a schematic of the node zone.

Insert deflection, slip

Insert microstrain, failure

Insert stress along bar, failure

3.2.2 SHEAR FAILURE SPECIMENS

3.2.2.1 CCT-#8-0.00X-8-U-6-S-1

This specimen was made in the regular CCT configuration with 2,800 psi concrete. Main reinforcement was a single #8 bar with no head. This beam was to be used as a control specimen. The beam was 8" wide, with the nodal area unconfined by shear reinforcement. The base plate was 6" in length, and this was the first test of its kind. **Figure 3.35** shows deflection under the load point. **Figure 3.36** shows that slip of the main reinforcing bar was not measured. **Figure 3.37** shows a plot of load versus microstrain. The bar shows yielding at the fifth strain gage. Throughout loading, certain areas of the cross section of the bar strain more than others. Strain readings, therefore, do not necessarily reflect the strain over the entire cross section of the bar. The bar continually adjusts, attempting to attain an even load distribution. This is shown when viewing results of SG Group 3, where one location along the bar has a strain gage on the top and one on the bottom of the bar. This specimen failed suddenly in shear. The maximum load experienced by the support under the node was 45.7 kips. **Figure 3.38** shows the failure shear crack on the south side of the beam. **Figure 3.39** shows a failure picture of the north side of the beam, stress along the bar, and a schematic of the strut-and-tie model.

Insert deflection, slip

Insert microstrain, failure

Insert stress along bar, failure

3.2.2.2 CCT-#8-0.00X-6-U-6-S-1

This specimen was made in the regular CCT configuration with 2,800 psi concrete. Main reinforcement was a single #8 bar with no head. The beam was 6" wide, with the nodal area unconfined by shear reinforcement. The base plate was 6" in length, and this was the first test of its kind. **Figure 3.40** shows deflection under the load point. **Figure 3.41** shows no slip behavior despite extensive splitting cracks. This data seems questionable because the cracking patterns indicate that slip activity was present. **Figure 3.42** presents load versus microstrain of the bar during testing. The fifth strain gage showed yielding around 42 kips. This specimen failed suddenly in shear at the maximum load of 49.2 kips and was accompanied by slight post-failure slip. This is shown by the splitting cracks along the bar and a small change in slip readings. **Figure 3.43** shows failure of the south side of the beam. **Figure 3.44** shows a failure picture of the north side of the beam, stress along the bar, and a schematic of the nodal zone.

Insert deflection, slip

Insert microstrain, failure

Insert stress along bar, failure

3.2.2.3 CCT-#8-5.34R-6-U-6-S-1

This specimen was made in the regular CCT configuration with 2,800 psi concrete. Main reinforcement was a single #8 bar with a 1.5"x3" rectangular friction-welded head. The beam was 6" wide, with the nodal area unconfined by shear reinforcement. The base plate was 6" in length, and this was the first test of its kind. **Figure 3.45** shows deflection under the load point. **Figure 3.46** shows some slip activity. **Figure 3.47** presents load versus microstrain of the bar during testing. The specimen failed suddenly in shear. The first signs of yield and maximum load of 66.9 kips occur simultaneously. There is significant post-failure yield activity. Splitting cracks have formed. The head confined the concrete and enabled the beam to carry higher load than the control specimen. **Figure 3.48** shows failure of the south side of the beam. **Figure 3.49** shows a failure picture of the north side of the beam, stress along the bar, and a schematic of the node zone.

Insert deflection, slip

Insert microstrain, failure

Insert stress along bar, failure

3.2.2.4 CCT-#8-0.00X-6-U-6-S-2

This specimen was made in the regular CCT configuration with 3,990 psi concrete. Main reinforcement was a single #8 bar with no head. The beam was 6" wide, with the nodal area unconfined by shear reinforcement. The base plate was 6" in length, and this was the second test of its kind. The specimen was unloaded and reloaded during the test due to equipment problems. **Figure 3.50** shows deflection under the load point. **Figure 3.51** shows significant slip of the main reinforcing bar. **Figure 3.52** presents load versus microstrain of the bar during testing. Yielding on the top of the bar at the fifth strain gage position began to occur at 46 kips. This specimen failed suddenly in shear immediately following bar slip at the maximum load of 53.7 kips. Yielding was only detected with SG5. **Figure 3.53** shows failure of the south side of the beam. **Figure 3.54** shows a failure picture of the north side of the beam, stress along the bar, and a schematic of the node zone.

Insert deflection, slip

Insert microstrain, failure

Insert stress along bar, failure

3.2.2.5 CCT-#8-2.17S-6-U-4-S-1

This specimen was made in the regular CCT configuration with 3,990 psi concrete. Main reinforcement was a single #8 bar with a 1.5"x1.5" square friction-welded head. The beam was 6" wide, with the nodal area unconfined by shear reinforcement. The base plate was 4" in length, and this was the first test of its kind. The specimen was unloaded and reloaded before failure due to inexact support alignment. **Figure 3.55** shows deflection under the load point. **Figure 3.56** shows slip of the main reinforcing bar. **Figure 3.57** presents load versus microstrain of the bar during testing. First yielding was recorded at 41.5 kips of load. This specimen failed suddenly in shear following bar slip at the maximum load of 43.4 kips. Some yielding of the bar occurred prior to failure. **Figure 3.58** shows failure of the south side of the beam. The beam has a piece missing because it fell to the side off of its supports immediately following failure. **Figure 3.59** shows a failure picture of the north side of the beam, stress along the bar, and a schematic of the node zone.

Insert deflection, slip

Insert microstrain, failure

Insert stress along bar, failure

3.2.2.6 CCT-#8-0.00H-6-U-4-S-1

This specimen was made in the regular CCT configuration with 3,990 psi concrete. Main reinforcement was a single #8 bar standard hook for anchorage. The beam was 6" wide, with the nodal area unconfined by shear reinforcement. The base plate was 4" in length, and this was the first test of its kind. The beam was unloaded and reloaded once due to equipment problems. **Figure 3.60** shows deflection under the load point. **Figure 3.61** shows slip readings for hooked reinforcing bar. The method of reading slip for this specimen seems to have been unsuccessful. This data is not reliable because there was a five inch difference in vertical placement of the potentiometers. This distance was too great because bending of the beam, then, affected beam behavior. **Figure 3.62** presents load versus microstrain of the bar during testing. First yield was detected at 51.8 kips. The specimen failed suddenly in shear at the maximum load of 51.8 kips. Some bar slip can be inferred from the cracking patterns along the failed specimen. This cannot, however, be verified from the flawed slip data. **Figure 3.63** shows failure of the south side of the beam. **Figure 3.64** shows a failure picture of the north side of the beam, stress along the bar, and a schematic of the node zone. Cracking along to the hook can be seen.

Insert deflection, slip

Insert microstrain, failure

Insert stress along bar, failure

3.2.2.7 CCT-#8-3.00H-6-U-4-S-1

This specimen was made in the regular CCT configuration with 3,990 psi concrete. Main reinforcement was a single #8 bar hook with no head. The beam was 6" wide, with the nodal area unconfined by shear reinforcement. The base plate was 4" in length, and this was the first test of its exact kind. **Figure 3.65** shows deflection under the load point. **Figure 3.66** shows slip of the main reinforcing bar. The method of reading slip for this specimen seems to have been unsuccessful. This data is not reliable because there was a five inch difference in vertical placement of the potentiometers. This distance was too great because bending of the beam, then, affected beam behavior. **Figure 3.67** presents load versus microstrain of the bar during testing. First yielding was detected at 46.0 kips. This specimen failed suddenly in shear at the maximum load of 49.0 kips. . Bar slip can be inferred from the cracking patterns along the failed specimen. **Figure 3.68** shows failure of the south side of the beam. **Figure 3.69** shows a failure picture of the north side of the beam, stress along the bar, and a schematic of the node zone.

Insert deflection, slip

Insert microstrain, failure

Insert stress along bar, failure

3.2.3 FLEXURAL YIELDING FAILURE SPECIMENS

3.2.3.1 CCT-#8-5.34R-8-U-6-S-1

This specimen was made in the regular CCT configuration with 2,800 psi concrete. Main reinforcement was a single #8 bar with a 1.5"x3" friction-welded head. The beam was 8" wide, with the nodal area unconfined by shear reinforcement. The base plate was 6" in length, and this was the first test of its kind. **Figure 3.70** shows deflection under the load point. The yield deflection before failure seems rather lengthy. **Figure 3.71** shows minimal slip of the main reinforcing bar. **Figure 3.72** presents load versus microstrain of the bar during testing. Yielding was first noted in the position of the fifth strain gage at 50.9 kips. The head prevented the bar from slipping and prevented shear failure. This specimen failed due to flexural yielding of the main reinforcing bar at the maximum load of 71.8 kips. **Figure 3.73** shows failure of the south side of the beam. **Figure 3.74** shows a failure picture of the north side of the beam, stress along the bar, and a schematic of the node zone.

Insert deflection, slip

Insert microstrain, failure

Insert stress along bar, failure

3.2.3.2 CCT-#8-11.68S-6-U-6-S-1

This specimen was made in the regular CCT configuration with 2,800 psi concrete. Main reinforcement was a single #8 bar with a 3"x3" square friction-welded head. The beam was 6" wide, with the nodal area unconfined by shear reinforcement. The base plate was 6" in length, and this was the first test of its kind. **Figure 3.75** shows deflection under the load point. **Figure 3.76** shows negligible slip activity. **Figure 3.77** presents load versus microstrain of the bar during testing. First yielding at the fourth strain gage occurred at 57.3 kips. This specimen failed due to yielding of the main reinforcing bar at the maximum load of 58.3 kips. Splitting cracks were formed along the bar. **Figure 3.78** shows failure of the south side of the beam. **Figure 3.79** shows a failure picture of the north side of the beam, stress along the bar, and a schematic of the node zone.

Insert deflection, slip

Insert microstrain, failure

Insert stress along bar, failure

3.2.3.3 CCT-#8-3.23R-6-U-4-S-1

This specimen was made in the regular CCT configuration with 3,990 psi concrete. Main reinforcement was a single #8 bar with a 1.5"x2" rectangular friction-welded head. The beam was 6" wide, with the nodal area unconfined by shear reinforcement. The base plate was 4" in length, and this was the first test of its kind. The beam was unloaded and reloaded several times due to problems with the data acquisition system. **Figure 3.80** shows deflection under the load point. **Figure 3.81** shows definite slip of the main reinforcing bar. This seems to have occurred post-failure. **Figure 3.82** presents load versus microstrain of the bar during testing. First yielding was detected at 50.5 kips at the sixth strain gage. This specimen failed due to yielding at the maximum load of 61.3 kips. **Figure 3.83** shows failure of the south side of the beam. **Figure 3.84** shows a failure picture of the north side of the beam, stress along the bar, and a schematic of the node zone.

Insert deflection, slip

Insert microstrain, failure

Insert stress along bar, failure

3.2.3.4 CCT-#8-3.90C-6-U-4-S-1

This specimen was made in the regular CCT configuration with 3,990 psi concrete. Main reinforcement was a single #8 bar with a threaded circular head. The yield stress for this specimen was 60 ksi, which is lower than the yield stress for the other specimens. The beam was 6" wide, with the nodal area unconfined by shear reinforcement. The base plate was 4" in length, and this was the first test of its kind. **Figure 3.85** shows deflection under the load point. **Figure 3.86** shows no slip of the main reinforcing bar. **Figure 3.87** presents load versus microstrain of the bar during testing. First yielding was detected at a load of 42.5 kips. The specimen experienced huge microstrains prior to failure and would not take load above 54.7 kips. This was considered failure. The head anchored the reinforcement well beyond the first signs of yielding. **Figure 3.88** shows failure of the south side of the beam. **Figure 3.89** shows a failure picture of the north side of the beam, stress along the bar, and a schematic of the node zone.

Insert deflection, slip

Insert microstrain, failure

Insert stress along bar, failure

3.2.4 COMBINATION FAILURE

3.2.4.1 CCT-#8-0.00X-6-U-4-S-1

This specimen was made in the regular CCT configuration with 3,990 psi concrete. Main reinforcement was a single #8 bar with no head. The beam was 6" wide, with the nodal area unconfined by shear reinforcement. The base plate was 4" in length, and this was the first test of its kind. **Figure 3.90** shows deflection under the load point. **Figure 3.91** shows some slip of the main reinforcing bar. **Figure 3.92** presents load versus microstrain of the bar during testing. No yielding occurred during the test. This specimen failed suddenly due to a combination of shear and diagonal compression strut failure at the maximum load of 42.3 kips. **Figure 3.93** shows failure of the south side of the beam. **Figure 3.94** shows post-failure cracking patterns on the north side of the beam. **Figure 3.95** shows a failure picture of the north side of the beam, stress along the bar, and a schematic of the node zone.

Insert deflection, slip

Insert microstrain, failure

Insert stress along bar, failure

3.2.4.2 CCT-#8-0.80C-6-U-4-S-1

This specimen was made in the regular CCT configuration with 3,990 psi concrete. Main reinforcement was a single #8 bar with a forged circular head. The beam was 6" wide, with the nodal area unconfined by shear reinforcement. The base plate was 4" in length, and this was the first test of its kind. During testing, a bad wire was detected. Therefore, the specimen was unloaded and reloaded before completing the test. **Figure 3.96** shows deflection under the load point. **Figure 3.97** shows some slip of the main reinforcing bar. **Figure 3.98** presents load versus microstrain of the bar during testing and shows no yielding. This specimen failed suddenly by a combination of shear failure and diagonal compression strut failure immediately following bar slip at the maximum load of 46.7 kips. **Figure 3.99** shows failure of the south side of the beam. **Figure 3.100** shows a failure picture of the north side of the beam, stress along the bar, and a schematic of the node zone.

Insert deflection, slip

Insert microstrain, failure

Insert stress along bar, failure

Chapter 4: Comparison of Test Results

4.0 INTRODUCTION

This chapter discusses the effects of the net head area to bar area ratio, the head shape, the specimen width, and the base plate length. It compares the slip, reinforcing strain, and failure mode of the specimens tested and relates the capacity to various failure expressions.

4.1 HEAD SIZE

The test specimens can be grouped for direct comparison according to specimen width, base plate length, and concrete compressive strength. Four 8" wide specimens with 6" base plate length and $f'_c = 2800$ psi were tested. The only variable in these specimens was A_h/A_b , which ranged from 0 to 11.68. Bar force was taken to be equal to the force at the support. This assumption was made according to STM because the diagonal compression strut was oriented at 45° with the horizontal. **Figure 4.1** shows the failure loads of this group of specimens. Failure was taken as the peak reaction at the support under the node. The dashed line designates the theoretical ultimate flexural capacity of the beams based on Grade 68 steel, which is 52.3 kips. **Figure 4.2** shows failure loads normalized with respect to the failure load of the non-headed bar, or control specimen. The control specimen failed in anchorage with some yielding. The lack of anchorage was probably a contributing condition to its failing at 87% of the calculated flexural ultimate load. The forged head specimen also failed in anchorage with some yielding, but carried 14% more load

insert figure 4.1, 4.2

than the control specimen. The 5.34R headed specimen reached stresses well beyond yield and carried 66% more load than the control specimen. The 11.68S headed specimen failed in anchorage after reaching strain hardening and carried 60% more load than the control specimen. Specimens with headed bars carried more load than the control specimen. The increase in capacity between the control specimen and the 5.34R headed bar specimen is significant. However, there is a decrease in capacity between the 5.34R and 11.68S headed bar specimens of about 3%, although the net head area to bar area ratio is over 50% higher. These tests indicate that capacity did not increase linearly with increase in head area to bar area ratio. The 11.68S head adds no capacity over the 5.34R head, although a head of approximately that size is required by the current ASTM-A970-98 [17] requirement, where the head area must be at least 10 times the bar area.

Three 6" wide specimens with $f'_c = 2800$ were tested with 6" long base plates. The A_h/A_b for these specimens ranged from 0 to 11.68. **Figure 4.3** shows the failure loads of this group. The dashed line indicates the theoretical ultimate flexural capacity of the beams, which is 50.6 kips. **Figure 4.4** shows normalized failure loads with respect to the failure load of the non-headed control specimen. The control specimen failed in anchorage with some yielding at 97% of the theoretical flexural capacity. The 5.34R headed bar specimen also failed in anchorage with some yielding but carried 36% more load than the control specimen. The 11.68S headed specimen yielded but carried only 19% more load

insert figure 4.3, 4.4

than the control specimen. All headed bar specimens carried more load than the control specimen. However, the capacity of the 11.68S headed bar specimen was unexplainably about 15% lower than that of the 5.34R headed bar specimen. Again, the results indicate that a head area approximately half of the 10 times the bar area, required by ASTM-A970-98, is sufficient.

Seven 6" wide specimens, $f'_c = 3990$ psi, were tested with 4" long base plates. The A_h/A_b for these specimens ranged from 0 to 3.90, and the group included two hooked bar specimens. **Figure 4.5** shows the failure loads of this group. The 3.90C headed bar specimen contained main reinforcement with 60 ksi yield strength, while all other specimens contained reinforcement with 68 ksi yield strength. The 3.90C specimen failed in flexural yielding. In order to make the 3.90C specimen directly comparable to the others in the group, the failure load was adjusted by the ratio of $68/60=1.13$ corresponding to yield strengths. The failure loads including the adjusted load of the 3.90C specimen are shown in **Figure 4.6**. The dashed line indicates the theoretical flexural ultimate capacity of the beams, which is 50.6 kips. **Figure 4.7** shows normalized adjusted failure loads with respect to the failure load of the non-headed control specimen. The control specimen failed in anchorage at 80% of the theoretical flexural capacity. The 0.80C forged head specimen also failed in anchorage but carried 11% more load than the control specimen. The 2.17S and 3.23R specimens failed in anchorage with some yielding and carried 3% and 45% more load than the control specimen, respectively. The 3.90C specimen yielded at an adjusted load 47% greater than that of the control specimen. The two specimens with hooked bars

insert figure 4.5, 4.6

insert figure 4.7

performed quite well. The 0.00H specimen, whose node location is along the straight part of the bar and is shown in **Figure 2.4**, carried 25% more load than the control specimen. The 3.00H specimen, whose node location is around the lower curved portion of the hook and is shown in **Figure 2.5**, had 16% more capacity than the control specimen. Although both hooked bar specimens had higher capacities than the control specimen, two of the headed bar specimens outperformed the hooked bar specimens. This is significant because headed bars are easier for construction and concrete placement. None of the bars used in this group of specimens met the A_h/A_b ratio of 10 requirements of ASTM-A970.

Figure 4.8 shows all anchorages and failure modes. Failure loads are plotted against A_h/A_b . The capacity trends are depicted with a dashed line. The capacity of the specimens increased nearly linearly with up to an A_h/A_b of about 5.3. Then, the behavior seemed to level out. The results indicate that the optimum A_h/A_b for the CCT node application tested is around 5 to 6. Headed bars with $A_h/A_b > 2.5$ outperformed hooked bars. More tests are needed with systematic isolation of variables to clarify the trends in behavior.

4.2 HEAD SHAPE

Specimens 3.23R with a rectangular head and 3.90C with a circular head were compared to determine the significance of head shape. The net head area to bar area ratios were within approximately 20% of each other. The failure load of the 3.23R specimen was 1% less than the adjusted failure load of the 3.90C specimen. Strain variations along the bar were very similar. The notable

insert figure 4.8

differences in behavior were slip activity and mode of failure. Specimen 3.23R experienced some slip, while specimen 3.90C did not. Slip may have been absent in the 3.90C because of the lower bar yield strength and therefore, lower actual failure load.

Circular heads are much easier to use in the field because no time has to be spent orienting the heads. Clear cover to the head is the same at any orientation. Rectangular and square heads may not meet minimum cover requirements, if they are not held in proper orientation, as shown in **Figure 4.9**. However, more tests are needed to determine the most favorable head shape and orientation. Although circular heads meet cover requirements with ease, the protuberances created by head shapes with corners may act to anchor headed bars against transverse bars much more effectively.

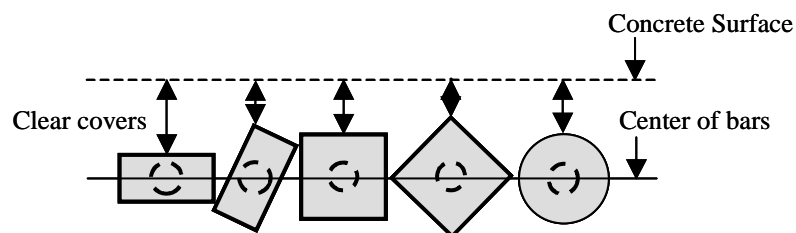


Figure 4.9: Clear Covers and Orientation of Headed Bars

4.3 SPECIMEN WIDTH

Pairs of specimens with no-heads, 5.34R, and 11.68S heads were compared to determine effects of a 2" difference in specimen width. All specimens had $f'_c = 2800$ psi and were tested with 6" base plate lengths. A

comparison of the failure loads is shown in **Figure 4.10**, with theoretical flexural failure loads indicated by dashed lines. According to flexure theory, an 8" specimen should have 3.5% more capacity than a 6" beam. Failure loads are normalized with respect to the 6" wide specimens for comparison and shown in **Figure 4.11**. The non-headed specimens failed in anchorage with some yielding at lower capacities than the theoretical flexural failure loads. The 6" wide non-headed specimen had 7% more capacity than the 8" wide non-headed specimen. The 8" wide 5.34R specimen had 13% more capacity than the 6" wide 5.34R specimen. The 8" wide 11.68S specimen had 30% more capacity than the 6" wide 11.68S specimen. The 6" wide 11.68S specimen failed by flexural yielding, which could have been caused by reinforcement with $f_y < 68$ ksi. The increase in capacity of the 8" compared with the 6" wide headed specimens indicates that the head was more efficient in the wider specimens. However, more tests are needed to quantify the effect of width. Wider specimens and specimens containing multiple bars should be tested.

4.4 BASE PLATE LENGTH

One pair of non-headed bar specimens was directly comparable for determining base plate length effects and is shown in **Figure 4.12a**. The normalized failure loads with respect to the specimen with the 4" base plate are shown in **Figure 4.12b**. The capacity with a 6" base plate length was 27% higher than with a 4" base plate. These tests seem reliable because the stresses are higher with a smaller support area, and the area of confinement created by the

Insert 4.10, 4.11

Insert 4.12a & b

base plate above the support is smaller coming from a smaller base plate. In addition, it can be inferred from the performance of the other specimens that the higher stresses and reduction in confinement caused by the shorter base plate length caused the ultimate capacity of the specimens to decrease. The 6" wide non-headed 4" base plate specimen with 3990 psi concrete carried 20% less load than the 6" base plate specimen with 2800 psi concrete even though the concrete compressive strength for the 4" base plate specimen was 43% higher.

Major cracks occurred from 2" to 5" along the length of the bar from the interior edge of the base plate. This seems to indicate that the critical sections and failure cracks in these specimens occurred the same distance from the inner edge of the base plate, regardless of the base plate length. It should also be determined if the support bearing effects would be significantly different if the supports were concrete columns monolithically cast with the beam rather than steel base plates. This would be a more practical condition in buildings.

4.5 SLIP ACTIVITY

Slip data were presented in Chapter 3. Three specimens yielded and showed no significant slip activity. The forged head specimen and the 2.17R headed specimen with base plate lengths of 4" experienced sudden slip activity. **Figure 3.12** shows this pattern of slip. The other specimens with slip data experienced gradual or gradual to sudden slip activity. **Figure 3.21** shows this gradual slip pattern. Slip at peak load is presented in **Figure 4.13**, and slip before losing all capacity is shown in **Figure 4.14**. Accurate slip readings were not obtained for two non-headed bar specimens and the two hooked bar specimens,

insert figure 4.13, 4.14

although crack patterns indicate the presence of slip activity. Slip is much larger for specimens with A_h/A_b less than 3, while specimens with higher A_h/A_b showed little or no slip. The three specimens with no measured slip had net head area to bar area ratios of 3.90 and higher. **Figure 4.15** shows force in the bar when the specimen reached 0.005" slip or showed no slip. Specimens with negligible slip activity are marked "No Slip." **Figure 4.16** shows the percentage of the specimen peak load when 0.005" slip occurred. Specimens with head ratios larger than 3 did not attain 0.005" slip until the load carried was above 90% of their peak load values. For non-headed specimens and specimens with head ratios smaller than 3, the range for occurrence of 0.005" slip was wider. They experienced slip of 0.005" at 85% to 100% of their peak loads. **Figure 4.17** shows force in the bar when the specimen reached 0.010" slip. **Figure 4.18** shows force in the bar when the specimen reached 0.04" slip. These figures show that specimens with the largest slip contained non-headed or headed reinforcement with head ratios less than 4.

Failure involving large slip is an undesirable failure mode. Although many of these specimens carried loads well above the predicted loads, as will be shown in Section 4.8, modes of failure involving anchorage failure must be avoided. This must be considered when creating guidelines that include node confinement. More tests are needed to determine the reliability of the results.

4.6 MEASURED BAR STRAINS

The test specimens were grouped according to specimen width, base plate length, and concrete compressive strength for a direct comparison of strains.

insert figure 4.15, 4.16

Insert figure 4.17, 4.18

Plots of strain along the length of the bar for the four 8" wide specimens are shown in **Figure 14.19**. Each series of strain readings shown occurred when yield strain was first detected by any of the strain gages along the bar in that specimen. Differences in development of the bar occurred as the head size varies. The non-headed bar and forged head bar had similar stress development along the bar. The development was small from 1" to 5", and it increased rapidly from 5" to 9". Differences in strain along the bar at first yield were roughly 2000 $\mu\epsilon$. A crack formed near the 7" location along the bar in the forged head specimen (0.80C), which explains the peak at that position. As A_h/A_b increased, strain activity of the bar became more gradual. Differences in microstrain along the bar at first yield were 1100 $\mu\epsilon$ for the 5.34R specimen and 900 $\mu\epsilon$ for the 11.68S specimen. As A_h/A_b increased from zero to 11.68, the strain gradient was flatter. Bearing on the head, therefore, significantly helped the bar to develop stresses in a short distance. It helped to avoid large peaks in stress that form at the critical section, which is discussed in Section 4.7. The fact that the strain gradient becomes flatter suggests that there is an optimal A_h/A_b less than 11.68. At 11.68, the head almost entirely developed or anchored the bar, and the deformations along the bar did not contribute much to its anchorage. It seems that an optimal head size might mobilize both bearing area of the head and deformations along the bar to develop the bar.

Strain along the length of the bar for the three 6" wide specimens with 6" base plate length made of 2800 psi concrete are shown in **Figure 14.20**. Unfortunately, some strain gages were damaged during casting. Therefore, the

insert figure 4.19, 4.20

information for this group is not as complete as desired. However, results obtained are in agreement with the behavior of the like head types shown in **Figure 14.19**. The series of strain readings shown occurred when yield was first detected by one of the strain gages in that particular specimen. The non-headed bar developed strains rapidly between 7" and 9". Strain patterns of the 5.34R and 11.68S specimens were very similar, with the strain gradient of the 11.68S bar being slightly less than that of the 5.34R specimen. The difference in strain between the 7" and 9" locations along the non-headed bar was roughly 1000 $\mu\epsilon$. Recorded differences in strain along the bar were 700 $\mu\epsilon$ for the 5.34R specimen and 200 $\mu\epsilon$ for the 11.68S specimen. This again shows that bearing on the head significantly aids in developing the bar over a short distance and reduces dependence on bar deformations for anchorage.

Microstrain readings at first yield from five 6" wide specimens with a 4" base plate length made of 3990 psi concrete are shown in **Figure 14.21**. Strain patterns are similar to those of the two previous groups shown in **Figures 14.19-20**. The series of microstrain readings shown occurred when yield was first detected by one of the strain gages in that particular specimen, except for the non-headed bar and forged head specimens. These specimens failed in anchorage. Therefore, the strains plotted for these two specimens are the largest that were experienced before failure. Development behavior of the bars can still be inferred from the plots. Strains rapidly increased along the non-headed bar specimen. The microstrain reading gradient was roughly 1800 $\mu\epsilon$. Just as for the forged head specimen in the first group, the non-headed and forged head readings for this

group showed a peak at the 7" location. This location appears to be the critical section, as is determined later in Section 4.7. The gradient for microstrain readings is around 1100 $\mu\epsilon$ for the forged head specimen. Although the head on the 2.17S specimen is small, it provides enough anchorage to allow strains of 1100 $\mu\epsilon$ at the 1" position along the bar. Development for this specimen largely occurred between the 1" and 5" locations and flattened between 5" and 9". The strain gradient was around 1300 $\mu\epsilon$. Again, there was a peak at 7" from the end of the bar. Strain behavior of the 3.23R and 3.90C specimens was almost identical and was more horizontal than in the other specimens. There was a decrease in strain at 5" for the 3.90C specimen. This decrease was probably due to localized conditions, such as cracking. Again, the head aided in reducing stress concentrations along the bar and allowing stresses to transfer more evenly. The headed specimens relied less on bar deformations for development. Gradients in microstrain readings along the bar for the 3.23R specimen are around 1200 $\mu\epsilon$ and 1400 $\mu\epsilon$ for the 3.90C, disregarding the reading at 5". This again shows that bearing on the head significantly aids in developing the bar over a short distance and reduces dependence on bar deformations for anchorage.

Strain along the bar of the two hooked bar specimens is shown in **Figure 14.22**. The 3" position along the bar in the graph corresponds to the point of tangency between the hook and the straight portion of the bar. The series of microstrain readings shown each occurred when first yield was detected in that particular specimen. As shown, the bars are fully developed by the hook. Strains are then uniform from the point of tangency down through the straight portion of

insert 4.21, 4.22

the bar. Like the larger headed bars, the hooked bars showed no large stress concentrations along the bar. The larger headed bar specimens carried significantly higher ultimate loads than the hooked bar specimens. In addition, congestion and construction problems are reduced when substituting larger headed bars for hooked bars.

In summary, the development behavior of non-headed and forged head bars was similar. Large stresses developed between 5" and 9" from the end of the bar and consequently on the outlying concrete adjacent to the bar deformations. With the addition of headed bars, higher stresses were developed closer to the head. This is advantageous because there is confinement occurring in the node that is not present at the critical section. Therefore, the high stresses are more easily resisted. Behavior of the larger headed bars was similar, as well, and did not significantly improve with the increase from an A_h/A_b of 5 to 11. The larger head provides enough bearing area for anchorage to reduce dependency on bar deformations. The bigger the head, the smaller the strain gradient along the bar. Therefore, large stress concentrations do not occur along the bar in specimens with larger heads.

4.7 DEVELOPMENT LENGTH AND DETERMINATION OF A CRITICAL SECTION

Development length and determination of a critical section were based on STM. The non-headed and smaller headed bars relied more upon bar deformations for force development within the bar, while the larger headed bars relied more on bearing of the head. Development length needed was further reduced by confinement. The base plate beneath the node and the intersection of

the two compression struts created confinement in all specimens. In the headed bar specimens, additional confinement was provided by the bearing area of the head. Additionally, the least amount of clear cover to the bar was 2.5". This is more cover than required for many construction purposes. Therefore, the confinement effect from the base plate seen in these tests is less than it would be for an actual application. In this regard, these tests are conservative.

The tests revealed information about the CCT node through strain readings, crack patterns and failure modes. If current AASHTO and ACI Code provisions for development length accurately described bar behavior for this CCT node, stress in a straight bar under the loading point at 18" from the end of the bar could not develop more than half of yield. Strain readings indicated that most bars yielded at 7" or 9" from the end of the bar. Some bars achieved yield strains 1" or 3" from the end of the bar. Although yield was detected extremely close to the end of the bar in some specimens, strain developed is not the only criteria for determining the critical section and development length. A certain embedment length must be present to enable the bearing area of the head to remain anchored and perform its function. Therefore, crack patterns were used to determine the necessary embedment length and hence, the critical section.

Figure 4.23 shows the nodal region of a typical specimen with the points along the bar that were considered in determining the critical section. The point along the bar directly under the load point was not chosen because flexural yielding was not the critical failure mode. The points at the face of the node and

insert figure 4.23

above the face of the support were discounted because most significant cracking took place further down the bar. Many of the specimens failed along cracks 2” down the bar from the inner edge of the base plate. However, shear cracks always formed first around 5” down the bar from the inner edge of the base plate, and that was chosen as the critical section to be conservative. The critical section is indicated with the dashed circle in **Figure 4.23**. Experimental development lengths were determined as the length from the end of the bar to the critical section and are listed in **Table 4.1**. The development lengths of these specimens are appreciably less than the current ACI Code and AASHTO Specification required development lengths.

4.8 ULTIMATE CAPACITY

Ultimate capacity of the beams was compared to existing theories on beam strength. None of the existing theories incorporate confinement conditions or confinement conditions coupled with head anchorages. Therefore, the theoretical failure loads are generally lower than the actual failure loads.

4.8.1 COMPARISON WITH ACI BUILDING CODE DEVELOPMENT LENGTH EQUATION

The advantage of confined and headed reinforcement can be seen when comparing actual stress achieved in the bars to calculated potential stress of a particular development length according to the development length equation in Chapter 12 of the ACI Building Code [12]. The basic development length equation is:

$$\frac{l_d}{d_b} = \frac{3}{40} \frac{f_y}{\sqrt{f'_c}} \frac{\alpha\beta\gamma\lambda}{\left(\frac{c + K_{tr}}{d_b}\right)} \quad (4-1)$$

where,

l_d = development length, in.

d_b = diameter of bar, in.

f_y = yield strength of bar, psi

f'_c = concrete compressive strength, psi

α = reinforcement location factor

β = coating factor

γ = reinforcement size factor

λ = lightweight aggregate concrete factor

c = spacing or cover to the centroid of the bar dimension, in.

K_{tr} = transverse reinforcement index

$$\left(\frac{c + K_{tr}}{d_b}\right) \leq 2.5$$

The yield stress, f_y , can be replaced with stress in the bar, f_s , and the equation can be manipulated to solve explicitly for f_s . The equation for bar stress as a function of development length is then:

$$f_s = \frac{40}{3} \frac{l_d}{d_b} \sqrt{f'_c} \frac{\left(\frac{c + K_{tr}}{d_b}\right)}{\alpha\beta\gamma\lambda} \quad (4-2)$$

Bar stresses were computed according to equation (4-2), using development length determined from test results. These are shown and compared to measured stresses in **Table 4.1**. All reinforcement reached the projected bar stresses, and all but the hooked bars achieved stresses 2 to 5 times the calculated values. Hooked bar specimens performed most closely to the calculated values. However, the code equation was still conservative in the case of hooked bars. This is not surprising because the equations contain an unstated factor of safety. Actual development lengths were roughly only 25% of the lengths required.

4.8.2 COMPARISON WITH AASHTO BASIC DEVELOPMENT LENGTH EQUATION

The development lengths achieved in these tests were significantly lower than those required by Section 8.25.1 of the AASHTO Standard Specifications for Highway Bridges [14]. AASHTO development length requirements are slightly more conservative those imposed by ACI. Confinement created by compression struts and bearing area of the head reduced the actual development length of the bar. The AASHTO basic development length requirement is:

$$l_d = \frac{0.04 A_b f_y}{\sqrt{f'_c}}, \text{ but not less than } 0.0004 d_b f_y \quad (4-3)$$

where,

l_d = development length, in.

A_b = cross-sectional area of bar, in.²

f_y = yield strength of bar, psi

f'_c = concrete compressive strength, psi

The can be manipulated to solve explicitly for bar stress. The equation for bar stress as a function of development length is then:

$$f_s = \frac{l_d}{0.04A_b} \sqrt{f'_c} \quad (4-4)$$

Table 4.1 shows comparisons of actual bar stress to calculated bar stress using equation (4-4). All measured stresses surpassed the AASHTO projected bar stresses by factors of again roughly 2 to 5, with a hooked bar being the lowest at 1.5. Actual development lengths were again about 25% of the lengths required.

4.8.3 COMPARISON WITH FLEXURE THEORY

Three of the tested specimens failed in flexural yielding. All other specimens but two experienced some yielding. Therefore, flexure theory was used to back-calculate ultimate failure loads for the specimens. The values obtained do not reflect development length or head anchorage factors. The following basic equation was used for this calculation:

$$M = A_s f_y \left(d - \frac{a}{2} \right) \quad (4-5)$$

where,

M = internal moment at the critical section, k-in.

A_s = cross-sectional area of bar, in.²

f_y = yield strength of bar, ksi

d = effective depth, distance from compression face to centroid of tension steel, in.

a = depth of Whitney rectangular stress distribution from compression face of beam, in.

Equation (4-5) can be manipulated to solve for the ultimate failure load of the specimen. The M term is replaced by a term containing the force at the support and a known moment arm. Because the diagonal compression strut was oriented at 45° with the horizontal, the force at the support was assumed to be equal to force in the bar. The force at the support is made explicit and substituted with the force in the bar. Finally, the known moment arm value is substituted:

$$F_s \cdot arm = A_s f_y \left(d - \frac{a}{2} \right)$$

$$F_s = \frac{A_s f_y \left(d - \frac{a}{2} \right)}{arm}$$

$$F_b = \frac{A_s f_y \left(d - \frac{a}{2} \right)}{15"} \quad (4-6)$$

F_s = force at the support, kips

F_b = force in the bar, kips

All failure loads computed are shown and compared with the actual failure loads in **Table 4.2**. Flexure theory significantly underestimates the failure loads of all

insert table 4.1

insert table 4.2

specimens that yielded. Seven of the other twelve specimens failed below the theoretical failure load. These specimens failed before reaching the yield load probably because the situation was not one of pure bending. Shear and anchorage were involved in the failure of the specimen, as well.

4.8.4 COMPARISON WITH DEVRIES SIDE-BLOWOUT EQUATION

DeVries developed a recommendation for side blowout behavior in his study of headed bars. He neglected the contribution of development length to the capacity for conservatism. Available area for failure, minimum cover, net head area to bar area ratio, and concrete strength were important in his determination. The recommended equation for determining side-blowout capacity of headed reinforcement is:

$$P_u = \frac{A_{bo}}{A_{bon}} 204.7 C_1 \sqrt{A_n f'_c} \quad (4-7)$$

where,

P_u = blow-out capacity, lbs.

C_1 = minimum edge distance to center of bar, in.

A_n = net bearing area of head, in.²

f'_c = concrete compressive strength, psi

A_{bo} = available failure area, in.²

A_{bon} = basic failure area, in.²

A_{bo} 's were 16"x14" for the 8" specimens and 13"x11" for the 6" specimens and were determined based on the recommendations of DeVries. **Figure 4.24** shows

the derivation of the A_{bo} . The Comité Euro-International du Béton (CEB) [22, 23] determined A_{bon} to equal $36C_1^2$, which was determined to be the average failure surface area of a single bolt near an edge. This value was used by DeVries in his study and in this comparison of failure loads. Force in the bar at failure was computed and is shown in **Table 4.2**. The DeVries equation underestimated the failure by about a factor of 2. This may be from neglect of the contribution from development length in the equation. More importantly, however, the significant contribution to capacity from confinement created by the compression struts and heads was shown.

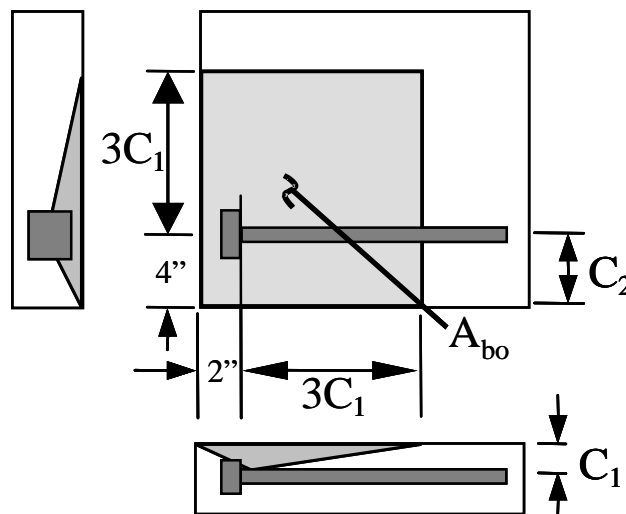


Figure 4.24: Failure Area for DeVries' Side Blowout

4.8.5 COMPARISON WITH ACI CODE CB-30

ACI Building Code Proposal CB-30 [13] offers recommendations for anchoring in concrete. This code provides guidance for conditions closer to those of these test specimens than other provisions. However, there is no guidance for anchorages in confined conditions.

Sideface blowout is covered by CB-30 as equation (D-11). The equation given is:

$$N_{sb} = 160c\sqrt{A_b}\sqrt{f'_c} \quad (4-8)$$

where,

N_{sb} = sideface blowout strength of a single anchor, lbs.

c = minimum edge distance to center of bar, in.

A_b = bearing area of the head of stud or anchor bolt, in.²

f'_c = concrete compressive strength, psi

If the perpendicular distance $c_2 < 3c$ from an edge, the value of N_{sb} must be multiplied by the factor $(1+c_2/c)/4$, where $1 \leq c_2/c \leq 3$.

Results from the calculations are shown and compared with actual failure loads in **Table 4.1**. Calculated failure loads are generally lower than actual failure loads by a factor of 2.

Equation (D-6a) predicts the basic concrete breakout strength of a single anchor in tension in cracked concrete. This was used for comparison with failure loads:

$$N_b = k\sqrt{f'_c} h_{ef}^{1.5} \quad (4-9)$$

where,

N_b = breakout strength, lbs.

k = coefficient for basic concrete breakout strength in tension,

$k = 24$ for cast-in anchors.

h_{ef} = effective anchor embedment depth, in.

The length of embedment to the critical section, or development length, was used in all calculations as h_{ef} . It is interesting to see that bearing area of the head is not a factor in the equation, yet the predicted failure loads were more accurate than any of the others calculated using CB-30 recommendations. All calculated failure loads were conservative, except for the two specimens that failed in anchorage, which were non-headed and had a 0.80C head.

In addition, the nominal concrete breakout strength of a single anchor in tension, given as equation (D-4a) of CB-30, was computed and compared to the failure loads. This equation considers cover and edge distance constraints. The equation is:

$$N_{cb} = \frac{A_N}{A_{No}} \psi_2 \psi_3 N_b \quad (4-10)$$

where,

N_{cb} = nominal concrete breakout strength in tension of a single anchor, lbs.

A_N = projected concrete failure area of an anchor or group of anchors, for calculation of strength in tension.

A_{No} = projected concrete failure area of an anchor or group of anchors, for concrete failure area of one anchor, for calculation of strength in tension, when not limited by edge distance or spacing. $A_{No} = 9 h_{ef}^2$.

Ψ_2 = modification factor, for strength in tension, to account for edge distances smaller than $1.5 h_{ef}$.

$$\Psi_2 = 0.7 + \frac{0.3c_{min}}{1.5h_{ef}}, \text{ if } c_{min} < 1.5h_{ef}$$

c_{min} = minimum edge distance to centroid of bar, in.

Ψ_3 = modification factor, for strength in tension, to account for cracking

$$\Psi_3 = 1.25 \text{ for cast-in anchors}$$

The derivation of A_N is shown in **Figure 4.25**. The test situation is unlike the conditions shown because the test specimen contains 3 rather than 2 limiting cover dimensions in the beam cross-section. The derivation of A_{No} is shown in **Figure 4.26**. Failure loads were calculated and are shown in **Table 4.2**. The use of development length as the effective anchor embedment, h_{ef} , makes the theoretical breakout load extremely conservative. The equation predicts the strength as if the reactions were far outside the beam, as shown with the solid arrows in **Figure 4.26**. However, a more accurate depiction of the true test conditions is shown with the dashed arrows, where the diagonal compression strut is in the immediate vicinity of the bar and creates confinement.

Insert figure 4.26, 4.27

The CCT node conditions do not fit well with any of the CB-30 equations. Confinement by struts and heads had a significant impact on ultimate capacity and anchorage. Therefore, guidelines must be developed for situations involving confinement at the node.

Chapter 5: Conclusions

5.1 SUMMARY

The use of headed reinforcement in concrete bridge applications offers a partial solution to construction and design problems related to placement and congestion of reinforcement in anchorage regions. Heads eliminate the need for standard hooks and embedment lengths. Use of headed bars in bridges, buildings, and traditional reinforced concrete construction is not widespread due to the lack of coverage in codes and specifications. Most application to date has been in offshore platform construction. Common use of headed bars is not likely until data is obtained for the development of design provisions.

The research conducted in this program focused on the application of headed bars in a typical structural detail – the support region of a beam. Test specimens were designed to study the performance of headed reinforcement in compression-compression-tension (CCT) nodal regions at the end of a beam. Strut-and-tie modeling was used to design the test specimen and to interpret behavior. Fifteen exploratory tests were performed on specimens with varying head size, head shape, specimen width, and base plate length. Mode of failure, failure load, deflection under the load point, slip of the bar, strain along the bar, and crack patterns were analyzed to determine trends in behavior.

5.2 CONCLUSIONS

From the data obtained, the following conclusions and observations were made about the performance of headed reinforcing bars in CCT nodal regions:

1) Anchorage capacity:

- a. Failure loads generally increased linearly as A_h/A_b ratios increased from 0 to 5.3. There was no further increase at A_h/A_b ratios of 11.68.
- b. Some specimens carried 15% to 45% more load than the predicted flexural capacity indicating that strain hardening was developed in the reinforcement.
- c. Specimens with 8 in. width carried between 7% to 30% higher loads than their 6 in. wide counterparts. The percentage increase was higher as the A_h/A_b ratio increased, although only three sets of specimens were compared.
- d. Failure load was not significantly affected by head shape, although only one set of specimens permitted a head shape comparison. Head shapes tested were circular, square, and rectangular. Circular headed bars have an advantage in that they provide the same clear cover regardless of orientation.
- e. Specimens with 6 in. base plates reached higher failure loads compared to specimens with 4 in. base plates, despite the fact that all specimens with 6 in. base plates had lower concrete compressive strength.
- f. The best overall performance was from the 5.34R headed bar. On average, it had 50% more capacity than the control specimen. It slipped less than 0.01" before failure and had a long yield plateau.

- g. Failures involving slip of the reinforcement were sudden and accompanied by nearly total loss of capacity.

2) Effective embedment lengths and strain variations:

- a. The critical section was determined to be around 10” from the end of the bar for specimens with 6” base plate length and 9.3” from the end of the bar for 4” base plate length specimens.
- b. Specimens with the 4 in. base plates experienced generally the same strain gradients before failure as specimens with the 6 in. base plates.
- c. Development for non-headed and forged bars with an A_h/A_b ratio of 0.80 involved large stress concentrations between 5 and 9 in. from the end of the bar. For headed bars with A_h/A_b ratios greater than 3, the majority of force in the bar was developed by the head bearing area. Large stress levels were developed immediately near the head, and there were only small variations along the bar toward the critical section. Hooks fully developed the bar at the point of tangency, however, the capacities of hooked bars were significantly less than those of headed bar specimens in comparable beams.

3) A number of design equations for straight, hooked, or headed bars were applied to the test specimens. All equations underestimated failure loads by about the ratios shown below. the given factors:

- a. ACI Development Length 4.0

b. AASHTO Development Length	4.0
c. DeVries Side-Blowout	2.0
d. CB-30 Side-Blowout	2.0
e. The CB-30 basic concrete breakout strength	1.5
f. The CB-30 nominal concrete breakout strength	10.4

These results are not surprising because none of the procedures include effects of confinement and restraint conditions similar to those of the test specimens.

5.3 RECOMMENDATIONS FOR FURTHER STUDY

The tests described in this thesis were exploratory. More testing is needed to verify the trends discussed and to determine the range of scatter generally associated with anchorage data. Variables must be isolated in order to quantify their contribution to the behavioral patterns. There was a gap in data for A_h/A_b ratios between 5.34 and 11.68. In addition, a maximum A_h/A_b ratio may exist, whereafter anchorage of such a large head may cause some undesirable localized effects. Tests allowing direct comparison between head shape should be performed. Tests involving specimens of width other than 6" or 8" should be considered. Tests with differing base plate lengths are needed to determine the location of critical sections. Because many of the tests were limited by yielding behavior, tests with larger bar sizes should be performed. These would offer more information about the behavior of the concrete struts and node. For general design procedures, the strut angle should be varied to determine its effects on behavior. Tests are needed with transverse reinforcement in the anchorage

region. Such reinforcement is typical in beam elements and will serve to increase confinement at the node.

BIBLIOGRAPHY

1. SINTEF Report No. STF20 F92020, “Static and Dynamic Pull-Out Tests of T-Headed Bars Embedded in Concrete,” SINTEF, Trondheim, Norway, 1992.
2. Berner, D.E., and Hoff, G.C., “Headed Reinforcement in Disturbed Strain Regions of Concrete Members,” Concrete International, Vol. 16, No. 1, January 1994, pp. 48-52.
3. Dr. Techn. Olav Olsen a.s., “Important Aspects for Further Development Concerning the use of T-Headed Bars in Concrete Design and Construction – Final Report” Norway, 1993.
4. DeVries, R.A., “Anchorage of Headed Reinforcement in Concrete,” PhD. Dissertation, The University of Texas at Austin, Austin, Texas, December 1996.
5. Bashandy, T.R., “Application of Headed Bars in Concrete Members,” PhD. Dissertation, The University of Texas at Austin, Austin, Texas, December 1996.
6. McConnell, Scott W., and Wallace, John W., “Behavior of Reinforced Concrete Beam-Column Knee-Joints Subjected to Cyclic Loading,” Report No. CU/CEE-95/07, Structural Engineering Research Laboratory, Department of Civil Engineering, Clarkson University, Postdam, NY, June 1995.
7. Ingham, J.M., “Seismic Design of Knee-Joints under Transverse Loading,” Applications of the T-Headed Bar in Concrete Design and Construction Workshop, St. John’s Newfoundland, 1994.
8. SEQAD Structural Engineers, Solana Beach, California, “Seismic Response of a Bridge Column/Cap-Beam Knee Joint Designed With Headed Reinforcement,” Report No. 95/12, Job No. 94/17, Prepared for Headed Reinforcement Corporation, Canada, 1995.
9. “Design of Fastenings in Concrete (Draft CEB Guide, Parts 1 to 3)” and “Fastenings for Seismic Retrofitting (State-of-the-Art Report on Design and Application),” Task Group 3.5 (Embedments), Euro-International Concrete

Committee (CEB), *CEB Bulletin D Information No. 226*, Comite Euro-International du Beton, August 1995.